JACS
JOURNAL OF THE AMERICAN CHEMICAL SOCIETY
Article
pubs.acs.org/JACS

Conservation and Functional Importance of Carbon−Oxygen Hydrogen Bonding in AdoMet-Dependent Methyltransferases

Scott Horowitz,[†,‡] Lynnette M.A. Dirk,[⊥] Joseph D. Yesselman,[‡] Jennifer S. Nimtz,[§,∥] Upendra Adhikari,[#] Ryan A. Mehl,[▽] Steve Scheiner,[#] Robert L. Houtz,[⊥] Hashim M. Al-Hashimi,[‡,§] and Raymond C. Trievel*[,∥]

[†]Howard Hughes Medical Institute, Ann Arbor, Michigan 48109, United States

[‡]Departments of Biophysics, [§]Chemistry, and [∥]Biological Chemistry, University of Michigan, Ann Arbor, Michigan 48109, United States

[⊥]Department of Horticulture, University of Kentucky, Lexington, Kentucky 40546, United States

[#]Department of Chemistry and Biochemistry, Utah State University, Logan, Utah 84322, United States

[▽]Department of Biochemistry and Biophysics, Oregon State University, Corvallis, Oregon 97331, United States

Supporting Information

ABSTRACT: *S*-Adenosylmethionine (AdoMet)-based methylation is integral to metabolism and signaling. AdoMet-dependent methyltransferases belong to multiple distinct classes and share a catalytic mechanism that arose through convergent evolution; however, fundamental determinants underlying this shared methyl transfer mechanism remain undefined. A survey of high-resolution crystal structures reveals that unconventional carbon−oxygen (CH···O) hydrogen bonds coordinate the AdoMet methyl group in different methyltransferases irrespective of their class, active site structure, or cofactor binding conformation. Corroborating these observations, quantum chemistry calculations demonstrate that these charged interactions formed by the AdoMet sulfonium cation are stronger than typical CH···O hydrogen bonds. Biochemical and structural studies using a model lysine methyltransferase and an active site mutant that abolishes CH···O hydrogen bonding to AdoMet illustrate that these interactions are important for high-affinity AdoMet binding and transition-state stabilization. Further, crystallographic and NMR dynamics experiments of the wild-type enzyme demonstrate that the CH···O hydrogen bonds constrain the motion of the AdoMet methyl group, potentially facilitating its alignment during catalysis. Collectively, the experimental findings with the model methyltransferase and structural survey imply that methyl CH···O hydrogen bonding represents a convergent evolutionary feature of AdoMet-dependent methyltransferases, mediating a universal mechanism for methyl transfer.

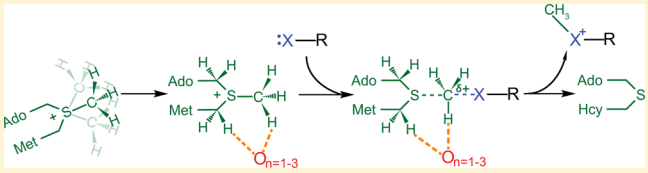

INTRODUCTION

S-Adenosylmethionine (AdoMet) is a versatile and ubiquitous enzyme substrate and is the most common methyl group donor in biology.[1,2] AdoMet-dependent methylation is essential to the metabolism of amino acids, cofactors, hormones, lipids, nucleic acids, and polysaccharides and has emerged as an important covalent modification of DNA and proteins, particularly with respect to epigenetic gene regulation. The enzymes that catalyze this reaction belong to as many as nine distinct classes that are unrelated by sequence, structure, or AdoMet binding modes.[3] Despite these differences, AdoMet-dependent methyltransferases share a conserved catalytic mechanism wherein the AdoMet methyl group is transferred to the acceptor substrate via an S_N2 reaction.[1,4] This reaction requires a linear alignment of the acceptor substrate (nucleophile), methyl group (electrophile), and the sulfur atom (leaving group) of the product *S*-adenosylhomocysteine (AdoHcy).[5] During the reaction, the methyl group inverts its stereochemistry, leading to a partially positively charged, sp^2 planar transition state. Currently, there are primarily three models as to how methyltransferases achieve their catalytic power: active site compression,[6] selective transition-state stabilization through hydrogen bonding and active site electrostatics,[7] and formation of a near attack conformation (NAC) between the electrophile and nucleophile.[5] It is conceivable that each of these mechanisms contributes at least in part to methyl transfer catalysis.

Recently, unconventional CH···O hydrogen bonds were demonstrated to coordinate the AdoMet methyl group in the active site of the SET domain class of protein lysine methyltransferases using NMR spectroscopy.[8] These interactions are generally thought to contribute about half the strength of a conventional hydrogen bond,[9] although computational and experimental studies indicate that the energy of these interactions can vary greatly and can have strengths equivalent to conventional hydrogen bonds, especially when the carbon is highly polarized or part of a charged group.[10,11] Although CH···O hydrogen bonding is ubiquitous in biomolecular structure and has been implicated in enzyme catalysis,[10−16] experimental evidence for the specific functions or importance of CH···O

Received: July 12, 2013
Published: September 6, 2013

   dx.doi.org/10.1021/ja407140k | *J. Am. Chem. Soc.* 2013, 135, 15536−15548

hydrogen bonding in biology is generally lacking. In the context of lysine methylation, these hydrogen bonds were hypothesized to perform several functions in lysine methyl transfer, including enhancing AdoMet binding, stabilizing the partially positively charged transition state and aligning the methyl group for optimal transfer geometry.[14] Here, we present data using an array of biochemical and biophysical approaches demonstrating that CH···O hydrogen bonds greatly augment AdoMet binding affinity and transition-state stability to a similar degree and constrain the motion of the AdoMet methyl group, possibly contributing to NAC formation.

EXPERIMENTAL SECTION

High-Resolution Crystal Structure PDB Survey. All cocrystal structures of methyltransferases bound to AdoMet with resolution better than 2.00 Å were downloaded and visually inspected before inclusion in the AdoMet and protein methyl and methylene CH···O hydrogen-bond surveys. Duplicate structures were removed, retaining the highest resolution structure of each methyltransferase. Electron density from the EDS server was examined to verify model quality when available.[17] Due to ambiguous $2F_o - F_c$ density corresponding to the AdoMet methyl group position, several structures (PDB accession codes 2IGT, 1FPX, 1I9G, 2EGV, 2QE6, 2YQZ, 3H6L, 3EEO, and 4DMG) were omitted from the survey. For certain structures (PDB accession codes 3UJ7, 1N2X, and 1ZQ9), analysis was restricted to a single copy of the methyltransferase, due to a lack of interpretable methyl group density. All other structures with multiple copies within the PDB file had CH···O hydrogen-bonding acceptor parameters averaged before analysis. Accession codes 1N2X, 2ZUL and 1V2X were refined by real space parameters using Coot[18] to adjust for model building and refinement anomalies before inclusion in the survey. In addition to AdoMet methyl and methylene groups, all protein side chain methyl and methylene C···O interactions were analyzed using identical hydrogen-bonding cutoffs to provide a reference point for analyzing the properties of the AdoMet methyl and methylene CH···O hydrogen bonds.

As methyl hydrogen positions for these structures were unknown, methyl group hydrogen bonding was based on van der Waals radii[12] and nonhydrogen atom angles. Four separate criteria were used to determine if methyl groups participated in CH···O hydrogen bonding: C···O distance, X−C···O angle, and C···O−Y angle, where X and Y are the nonhydrogen atoms bonded to carbon and oxygen, respectively, and sp^2 oxygen−methyl elevation angle.[19] Hydrogen bonding was determined using two scenarios: (1) For C···O distances <3.25 Å, which is the sum of the van der Waals radii of carbon and oxygen; and (2) for distances ≥3.25 Å but <3.70 Å, which is the combined van der Waals radii of a C−H bond and oxygen arranged in linear geometry.[12] In the former scenario, methyl groups were considered to participate in CH···O hydrogen bonding if the C···O distance was <3.25 Å, the X−C···O angle was between 60° and 160°, and the elevation angle was <75°. For the latter scenario, methyl groups were considered to undergo CH···O hydrogen bonding if the C···O distance was <3.70 Å, the X−C···O angle was between 85° and 140°, and the elevation angle was <50°. The C···O−Y angle was required to be >90° or between 75° and 160° for sp^2- or sp^3-hybridized oxygen atoms, respectively. In-house software to measure methyl hydrogen-bonding criteria was written using MATCH API to manipulate atoms.[20] Based on this criterion, ∼28% of the protein methyl groups surveyed exhibited CH···O hydrogen bonding. Protein methyl groups clearly favor relatively long CH···O interactions (mean of 3.8 Å), consistent with previous investigations of unpolarized methyl CH···O hydrogen bonding in small molecules.[21] Distance and angular distributions were volume corrected by multiplying the counts by $1/r^3$ and $1/\sin\theta$, respectively.[22] Distributions of angles and distances were analyzed using Origin (OriginLab).

To calculate whether the AdoMet methyl CH···O hydrogen bonds were significantly different from that of protein methyl groups, we examined the average length of each of the two populations. The difference between the mean lengths of each population was determined to be 0.31 Å. To establish whether this difference is significant, we recombined both populations and used the Fisher−Yates algorithm[23] to randomly reorder the data set, followed by division into two subsets containing the same number of hydrogen-bonding interactions as the two original populations (127 and 9881 members, respectively) and the difference between average lengths calculated. This process was repeated 100 000 times, generating a normal distribution with an average difference of 0.025 Å and standard deviation of 0.019 Å. These values yield a Z-score of 15.2σ or a confidence value >99.999%, permitting us to reject the null hypothesis.

In addition to methyl groups, all AdoMet and protein methylene CH···O hydrogen bonds were measured and volume corrected as described above for methyl groups, with the exception that hydrogen atoms were modeled into the riding positions using Chimera[24] and used to define CH···O hydrogen bond angles. In addition to the longer distance (<3.70 Å) and the same sp^2 oxygen angles defined above, the C−H···O angle was required to be between 110° and 250° for sp^3 oxygens and between 100° and 260° for sp^2 oxygens, with a maximum hydrogen elevation angle with the sp^2 oxygen plane of 60°.

Synthetic Peptides and Protein Expression and Purification. TAF10 peptide (Ac-SKSKDRKYTL-amide), TAF10 K189A (Ac-SKSADRKYTL-amide), and TAF10-biotin peptide (Ac-SKSKDRKYTLT(KEZLinkSSBiot)-amide) with S−S linker (Pierce) were obtained from New England Peptides. Peptide concentration was determined using tyrosine absorbance at 274 nm^{-1} (ε = 1.399 M/cm^{-1}). Wild-type (WT) SET7/9 and SET7/9 Y335F were expressed and purified as described previously.[8,25]

X-ray Crystallography. WT and Y335F SET7/9 crystals were grown by hanging drop vapor diffusion at 20 °C, as previously described[26] with the following exceptions: crystallization solution was mixed in a 1:1 ratio with 10−12 mg/mL enzyme, 6 mM AdoMet or 3.0−4.5 mM AdoHcy, and 2.0 mM of a 10-residue peptide of TAF10 peptide or TAF10 K189A peptide in 20 mM Tris pH 8.0, 100 mM NaCl, and 2.0 mM Tris(2-carboxyethyl)phosphine. Crystallization solutions contained 0.86−1.07 M sodium citrate with 100 mM imidazole, pH 7.6−8.4 and 8.0−18 mM $NiCl_2$. Y335F crystals were flash frozen in 1.5 M sodium citrate with 1.0 mM AdoHcy, 10−13 mM $NiCl_2$, and 100 mM imidazole pH 8.2−8.7 after 2 days of crystallization time. For WT SET7/9, crystals were flash frozen in the same cryoprotectant, omitting AdoHcy, 16−28 h after setup to obtain the AdoMet complex and 3−5 weeks after setup for the AdoHcy complex. Data were collected at the Advanced Photon Source Synchrotron beamline 21-IDG (LS-CAT), at 100 K and wavelength 0.9786 nm, and were processed using HKL2000.[27] The structures were solved by molecular replacement using MOLREP,[28] with the previously reported protein coordinates of the SET7/9 ternary complex (PDB accession code 3M53) and AdoMet-bound complex (PDB accession code 1N6A)[26,29] as the search models. Model building and refinement were carried out using Coot[18] and REFMAC,[30] respectively. The quality of the final models was verified by Molprobity.[31] CNS was used to generate simulated annealing omit maps for each of the different structures.[32] In the SET7/9 Y335F structure, K189, Phe-335, and AdoHcy were omitted. In each of the WT SET7/9 structures, His-293, Gly-264, Tyr-335, AdoMet, and AdoHcy were omitted. RMSD values were calculated, and structural figures rendered in PyMOL (Schrödinger, LLC).

Isothermal Titration Calorimetry (ITC). SET7/9 Y335F·TAF10 peptide ITC experiments were performed using a MicroCal VP-ITC calorimeter (GE Healthcare), as previously described for WT SET7/9 with identical buffer and temperature conditions.[26] Stoichiometry constants were equal to 0.8 for the SET7/9 Y335F·TAF10 peptide interactions.

Intrinsic Fluorescence Binding Assays. The weak AdoMet and AdoHcy affinities displayed by the SET7/9 Y335F mutant precluded analysis of their binding constants by ITC. To measure cofactor binding to the Y335F mutant, a fluorescence binding assay was developed that presumably quantifies the change in intrinsic fluorescence of active site Trp352 that stacks adjacent to the cofactor adenine ring.[29] Dissociation constants for AdoMet and the product

AdoHcy were calculated using intrinsic fluorescence measurements in triplicate using a Safire II plate reader (Tecan Group Ltd.) and round-bottom, black Costar 96-well plates (Corning). Buffer conditions were identical to previous SET7/9 ligand binding studies by ITC (20 mM sodium phosphate pH 7.0 and 100 mM NaCl).[8] Varying concentrations of ligand were added to 1.75 μM of SET7/9 Y335F, and fluorescence monitored between 320 and 390 nm at 37 °C after excitation at 280 nm. The measured fluorescence change was ∼3−5 fold, depending on the enzyme and ligand used. Resulting fluorescence profiles were fit to a Gaussian function, and then calculated amplitudes were plotted as a function of ligand concentration, and dissociation constants determined by fitting in Prism (GraphPad) and SigmaPlot 11.0 (SigmaPlot). The fraction bound was determined by using the fitted saturation point of each individual experiment as equal to 1.0. For certain experiments, nonspecific binding was additionally observed, as evidenced by a linear trend at high ligand concentration. This nonspecific binding was subtracted out using a linear fit model. Resulting binding curves were verified to produce dissociation constants within error of those calculated using a fitting model with a linear nonspecific binding term included in the fitting procedure. When measured separately, neither ligand nor SET7/9 showed discernible fluorescence change with increasing concentration. Comparing ITC and fluorescence data, the dissociation constants for AdoHcy and WT SET7/9 (60 ± 5[8] and 134 ± 36 μM by ITC and fluorescence experiments, respectively) differed by only 2-fold.

Differential Scanning Calorimetry (DSC). Melting enthalpy and temperatures of WT SET7/9 and SET7/9 Y335F were measured using a nanoDSC calorimeter (TA Instruments), with a scan rate of 1 °C/min from 18° to 100 °C at 3 atm constant pressure and a sample concentration of 0.9 mg/mL protein. Buffer conditions were identical to binding assay conditions. Data were analyzed using nanoAnalyze software (TA Instruments), and the figure was prepared using Origin 8.5 (OriginLab).

NMR Spectroscopy. 2D NMR and spin-relaxation experiments on WT SET7/9·AdoMet and SET7/9 Y335F·AdoMet were carried out on a 600 MHz Avance Bruker NMR spectrometer equipped with a triple resonance cryoprobe at 298 K. The SET7/9 Y335F sample used for chemical shift determination contained 0.1 mM $^{13}CH_3$-AdoMet (generated as previously described)[8] and 1.0 mM SET7/9 Y335F to enable saturation of the cofactor by enzyme. $^{13}CHD_2$-AdoMet experiments were performed in: 20 mM sodium phosphate, pH 7.5, 100 mM NaCl, and 0.5 mM TCEP in 98% D_2O. $^{13}CHD_2$-AdoMet was enzymatically synthesized from $^{13}CHD_2$-methionine and ATP as previously described.[8] NMR data were processed using NMRPipe/NMRDraw[33] and iNMR (www.inmr.net) and analyzed using Sparky.[34]

^{13}C relaxation rates were determined using $^{13}CHD_2$-AdoMet and a perdeuterated protein sample (see above), with a constant $R_1\rho$ spin-lock power of 3500 Hz to eliminate any R_{ex} contributions. ^{13}C relaxation rates were measured using pulse sequences[35,36] that were modified to incorporate deuterium decoupling for the duration of the experiments, as previously described.[37] WT SET7/9 correlation time (21 ns) was calculated from its structure (1N6A)[29] using HYDRONMR[38,39] and D_2O viscosity of 1.100 cP.[40] Relaxation rates were analyzed as previously described,[41] with the exception that the methyl C−H distance was set to 1.08 Å, based on our quantum chemistry optimizations of the AdoMet methyl group in the presence of a CH···O hydrogen-bonding partner, using in-house written software that incorporates spectral density analysis into an extended Model-Free formalism.[35] Due to the inability to generate stable perdeuterated SET7/9 Y335F, we were unable to measure relaxation data on the mutant SET7/9. Relaxation data was fit using Prism 5 (GraphPad).

Order parameters for AdoMet bound in the active site of methyltransferases were calculated for AdoMet molecules using the same structures as the PDB survey. AdoMet molecules were aligned by the sulfur and two adjacent methylene carbon atoms using the alignment protocol in PyMOL (Schrödinger, LLC). Free AdoMet order parameters were calculated from a 10 ns MD simulation of AdoMet previously verified to correctly model the methyl group electronic environment.[8] The AdoMet molecules in the MD simulation were aligned by the center of mass of the same three atoms as above, followed by an exhaustive rotation search. Order parameters were calculated from these ensembles as previously described.[42,43]

Radiometric AdoMet Assays. Purified WT SET7/9 (0.06−0.25 μM) and the Y335F mutant (0.3 μM) were used in duplicate steady-state methyltransferase assays[44] with biotinylated TAF10 peptide (2 mM).[26] Assays contained 25 mM NaCl, 100 mM bicine pH 9.0, and various concentrations of [^{3}H-methyl] AdoMet (Perkin-Elmer) diluted to specific activities from 0.16 to 3.6 μCi/nmole (original specific activity 55−85 Ci/mmol) with purified AdoMet[45] in a final volume of 20 μL and incubated at 37 °C. Assays were terminated at 1 and 2 min for WT SET7/9 and SET7/9Y335F, respectively (rates measured were linear over these times), by addition of an equal volume of 7 M acetic acid prior to addition of a 2-fold molar excess of immobilized streptavidin resin (UltraLink; Pierce Biotechnology, Inc.). After 30 min at room temperature for binding of the peptide, the resin was collected in a filter unit by centrifugation, washed three times with 300 mM NaCl, and transferred to a microtube with 0.8 M TRIS, pH 8.0, and 0.1 M TCEP for overnight vortexing to elute the peptide. Measurement of tritium incorporation during the assay was performed the following morning by liquid scintillation spectroscopy. For each activity determination, two separate control assays (without enzyme and without peptide substrate) were conducted in concert for background correction. Data were plotted and then fitted to the Michaelis−Menten equation using SigmaPlot 11 (Systat Software, Inc.).

Single turnover assays were performed using identical conditions as above for assays regarding temperature and processing. Assays were conducted with 60 μM AdoMet (60 μM; 4.7−6.3 μCi/nmole), 70 or 140 μM enzyme, and 1 or 2 mM biotinylated TAF10 peptide. Under these conditions, the ternary complex of SET7/9·AdoMet·TAF10 peptide is close to fully saturated, and all of the AdoMet is consumed. We observed that increasing either the enzyme or peptide concentration by 2-fold had no significant (≤30%) effect on the rate constant, suggesting that the maximal single turnover rate constant was determined. Assays were video recorded to allow frame-by-frame analysis using a trial version of Smart Cutter for DV and DVB (FameRing Co. Ltd.; http://www.fame-ring.com/smart_cutter.html) to determine the exact length of each assay. Data were plotted and then fitted with the single exponential curve using OriginPro 8.5 (OriginLab).

Quantum Chemistry Calculations. Calculations were carried out via the Gaussian 09 package[46] using the M06-2X variant of density functional theory[47] with a 6-31+G** basis set in gas phase. This approach was applied in part so as to better characterize intermolecular interactions of the sort being considered here and has enjoyed good success in the past.[48−56] Structures were identified as minima via the presence of all positive harmonic frequencies. All interaction energies were corrected for basis set superposition error by the counterpoise procedure.[57] To gauge the accuracy of M06-2X/6-31+G**, its binding energies were compared to MP2/aug-cc-pVDZ, which is considered quite reliable. The SMe_3^+ cation, very similar to the $SMe(Et)_2^+$ examined here, was allowed to bind with NMA, in a fully optimized structure. The binding energy calculated for this complex at the M06-2X/6-31+G** level was found to be 22.2 kcal/mol, only slightly larger than the value of 20.1 obtained with the benchmark MP2/aug-cc-pVDZ calculations. Moreover, prior calculations had suggested that if the level of theory were to be raised even higher, beyond MP2/aug-cc-pVDZ[58] the binding energy would increase slightly, thus bringing M06−2X/6-31+G** even closer in line with the best calculations possible.

RESULTS

Methyltransferase Survey. A previous study illustrating that CH···O hydrogen bonds are conserved in the active sites of SET domain lysine methyltransferases prompted us to examine whether CH···O hydrogen bonds are present in other methyltransferase classes.[11,14] A survey of 46 high-resolution

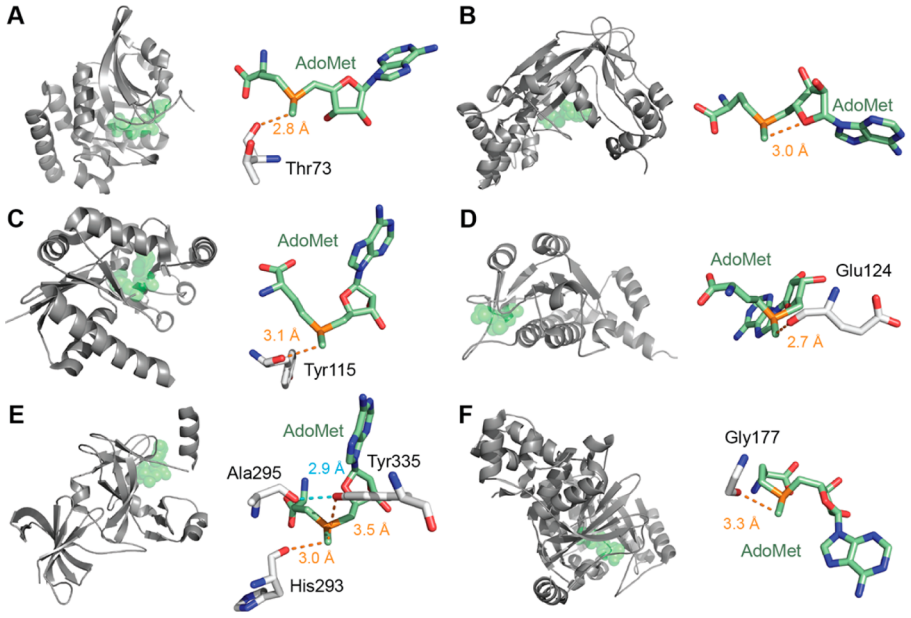

Figure 1. Representative examples from six classes of AdoMet-dependent methyltransferases illustrating inter or intramolecular CH···O hydrogen bonding (orange dashed lines) to the AdoMet methyl group. The hydrogen-bond donor and methyl C···O interaction distances are labeled in each enzyme. (A) Class I (Rossmann fold-like): L-isoaspartyl *O*-methyltransferase (PDB accession code 1JG4);[59] (B) Class II: Methionine synthase reactivation domain (1MSK);[60] (C) Class III: CobF precorrin-6A synthase (2NPN); (D) Class IV (SPOUT): TrmH tRNA 2′-*O*-methyltransferase (1V2X);[61] (E) Class V (SET): SET7/9 lysine methyltransferase (1N6A);[29] and (F) Class VI (Radical SAM): RlmN rRNA adenosine methyltransferase (3RFA).[62] Other known methyltransferase classes also appear to have the potential for CH···O hydrogen bonding to AdoMet but currently lack high-resolution structures in complex with AdoMet.[63−65]

crystal structures (<2.0 Å resolution) of AdoMet-dependent methyltransferases using typical CH···O hydrogen-bonding cutoffs[12] (Experimental Section) encompassing all of the major classes revealed that 44 structures display clear evidence of at least one CH···O hydrogen bond to the AdoMet methyl group (Figure 1A−F, Table S1). Notably, the two outstanding structures had C···O contacts whose distance were either well within the refinement coordinate error of the survey cutoff distance (PDB accession code: 1VPT), or missed the strict angular cutoffs by <1.5° despite having a 3.3 Å C···O contact distance (4DF3). Of the structures surveyed, one-half exhibit multiple AdoMet methyl CH···O hydrogen bonds. Many of these interactions are closer than 3.25 Å, the van der Waals contact distance between a carbon and an oxygen atom without an intervening hydrogen atom (Figure 2A). This observation is unsurprising given that atoms that participate in conventional hydrogen bonding, such as oxygen and nitrogen, frequently display hydrogen bond distances shorter than their van der Waals contact distances.[12] Additionally, we found that in every methyltransferase surveyed, at least one of the AdoMet methylene groups adjacent to the sulfonium cation engages in hydrogen bonding (Figure 2B). It is notable that the distribution of C···O interaction distances for both the AdoMet methyl and methylene groups are substantially shorter than equivalent distances derived from protein side chain methyl and methylene groups analyzed in the same set of structures (Figure 2A,B).

To gain insight into the nature of the AdoMet CH···O interactions, we compared the stereochemical parameters of CH···O hydrogen bonding to the AdoMet methyl and methylene groups to those of protein methyl and methylene groups in the same set of methyltransferase structures (Figure 2). The distribution of angles for all protein methyl groups displays a modest tendency toward coplanarity (Figure 2C), in contrast to the AdoMet methyl group that exhibits stringent coplanarity (Figure 2C). This observation implies that AdoMet methyl CH···O hydrogen bonding is stronger than analogous interactions formed by protein methyl groups. The combination of short C···O interaction distances and a strong tendency toward coplanarity observed for AdoMet methyl hydrogen bonding is inconsistent with typical weak methyl CH···O hydrogen bonding.[66,67] A similar analysis for the AdoMet methylene groups yielded a different trend. Unlike its methyl group, the AdoMet methylene groups behave very similarly to protein methylene groups (Figure 2D). This finding suggests either that the AdoMet methylene groups do not form uniquely strong CH···O hydrogen bonds compared to other methylene groups or that there is a different functional role for the methylene hydrogen bonds that does not necessitate planarity. It is also conceivable that this reflects a difference in our confidence in the positions of the hydrogen atoms in question, as hydrogen atoms can be less confidently modeled for methyl groups in contrast to methylene groups that are bonded to two heavy atoms.

Quantum Mechanical Calculations of CH···O Hydrogen-Bond Energies. Having observed AdoMet CH···O hydrogen bonds uniformly across methyltransferase crystal structures, we next assessed whether these interactions are energetically stabilizing. As the most common hydrogen-bond acceptors found in the survey were backbone carbonyl groups and tyrosine hydroxyl groups, we used quantum mechanical (QM) calculations to evaluate the strength of these interactions with the methyl and methylene groups of the sulfonium cation in AdoMet. To model these interactions, we employed a $SMe(Et)_2^+$ cation to mimic the AdoMet hydrogen-bond donors and either phenol or *N*-methylacetamide (NMA) for the oxygen acceptors.

dx.doi.org/10.1021/ja407140k | J. Am. Chem. Soc. 2013, 135, 15536−15548

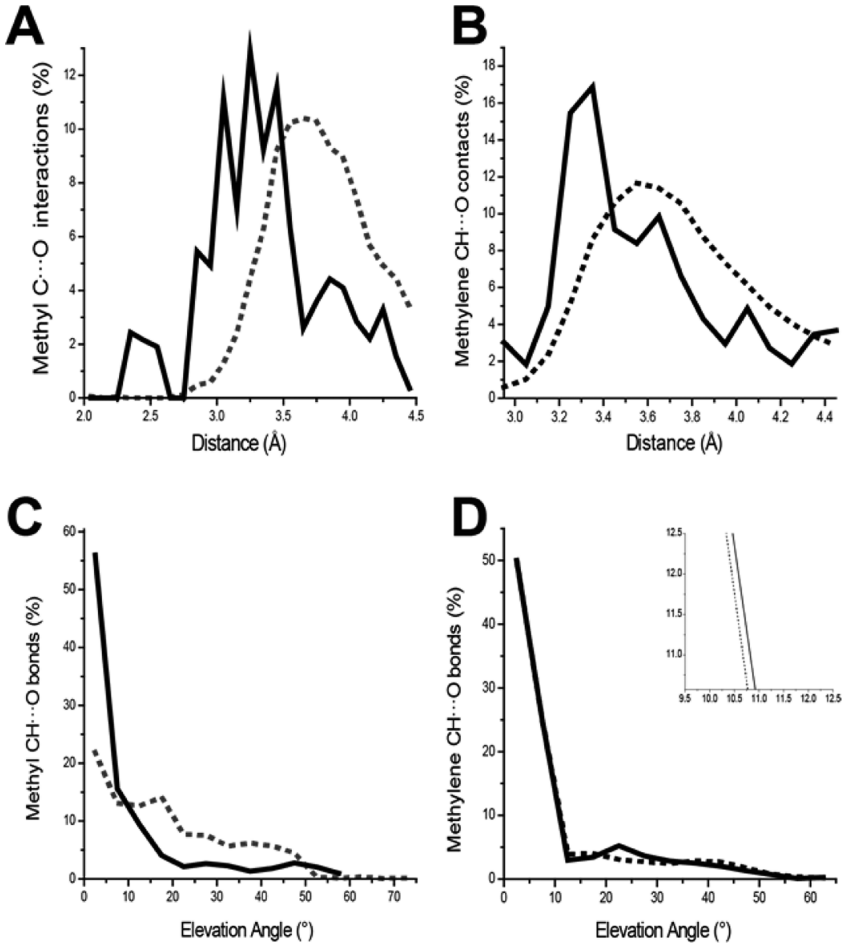

Figure 2. Distance and angular distribution of methyl and methylene CH···O hydrogen bonding in AdoMet-dependent methyltransferases. Overlay of normalized histograms of (A) methyl and (B) methylene group-oxygen distances for AdoMet (solid line) and protein methyl groups (dashed line) that satisfy hydrogen-bonding angular criteria (Experimental Section). Diagrams of elevation angles of (C) methyl and (D) methylene groups with C···O interaction distances <3.7 Å that satisfy hydrogen-bonding angular criteria (Experimental Section). Inset displays overlapped region between 9.5° and 12.5°.

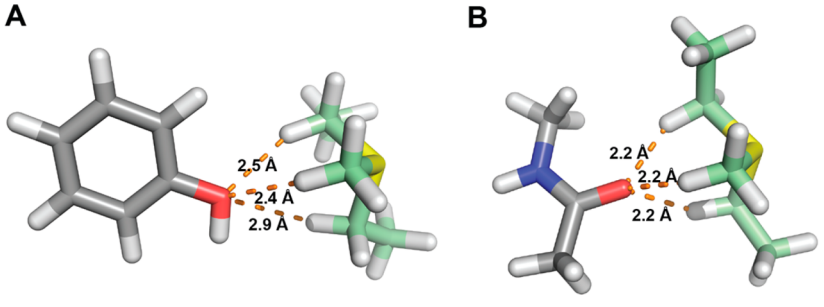

Figure 3. Optimized CH···O hydrogen-bond distances of model AdoMet, $SMe(Et)_2^+$, to phenol with energy of 7.4 kcal/mol (A) and *N*-methylacetamide with energy of 20.5 kcal/mol (B). H···O interaction distances are shown.

When paired with phenol, the $SMe(Et)_2^+$ cation formed quite a number of different minima when allowed a full optimization, 26 to be exact. The most stable of these minima is bound by 13.8 kcal/mol, with the phenolic oxygen forming a pair of CH···O hydrogen bonds to the ethyl group, both <2.7 Å in length (Figure S1). The other ethyl group engages in a CH···π hydrogen bond to the π-cloud of the phenyl ring. A scan of the other minima on the potential energy surface of this pair leads to the conclusion that the latter CH···π interaction is a common theme, along with various different CH···O hydrogen bonds. This observation is unsurprising in light of the negative electrostatic potential above the phenyl ring that would naturally attract the partially positively charged CH protons. The entire set of minima on the surface range in binding energy from the maximum of 13.8 to a minimum of 7.8 kcal/mol (Figure S1). Within the set of fully optimized minima, the one that appeared to have the lowest degree of CH···π bonding was 24th in energetic order. This structure appears to derive its binding energy of 9.7 kcal/mol exclusively from the two (or possibly three) CH···O hydrogen bonds to the phenolic oxygen atom. Because the structural restraints of the biological system do not allow the approach of the CH bonds

dx.doi.org/10.1021/ja407140k | J. Am. Chem. Soc. 2013, 135, 15536−15548

toward the aromatic system, two different sorts of restraints were imposed. In the first, the θ(S···O−C) angle connecting $SMe(Et)_2^+$ to the phenol was held at 180°, and the remaining parameters fully optimized. Without the possibility of a CH···π interaction, the binding energy is reduced to 7.2 kcal/mol. This binding can be attributed entirely to the two rather strong CH···O hydrogen bonds to the phenol oxygen atom. A second means of ensuring that the binding is purely a matter of CH···O hydrogen bonding is to hold the far end of the phenol unit (the C para to OH) at a fixed distance of 7.80 Å from the S atom (Figure 3A). This distance was chosen to match that observed in the crystal structure of SET7/9 (PDB accession code 1N6A), which was previously confirmed to form CH···O hydrogen bonds to the AdoMet methyl group. Again, a full optimization of all other parameters led to the structure below, which contains at least two, and perhaps three, CH···O hydrogen bonds to the phenol oxygen. The binding energy of this structure is 7.4 kcal/mol, quite similar to the one above with the fixed angular constraint. So one can conclude that the binding of the phenol O to the various CH groups of the cation, without the benefit of any other attractive forces such as CH···π, amounts to some 7−9 kcal/mol.

The most common hydrogen-bond acceptor found in the survey is the carbonyl oxygen atom of peptide bonds and is modeled here by NMA. As the electrostatic potential of the latter molecule contains only one negative region, around the oxygen atom,[68] one might expect fewer possible minima than phenol. Indeed, only four minima were identified on the surface. All four structures are characterized by CH···O hydrogen bonds, differing only in a few details. For example, the most stable (Figure 3B) is bound purely by three CH···O hydrogen bonds, all ∼2.2 Å in H···O length and C···O interaction distances of 3.1−3.2 Å. The three participating protons reside on the methyl group and on the methylenes of the two ethyl groups. Notably, this orientation of AdoMet to a backbone carbonyl group was very common in the survey. This interaction in total amounts to 20.5 kcal/mol, considerably stronger than the case where phenol serves as proton acceptor. The next most stable dimer contains only two such CH···O, again to the two methylene groups, and is only 0.3 kcal/mol less stable than the global minimum (Figure S2). If, on the other hand, all CH···O hydrogen bonds derive from the same ethyl group, there is a loss in stability by some 5−6 kcal/mol. Even so, the corresponding minimum is still bound by 14.3 kcal/mol.

To place these interaction energies into context, one can consider the usual paradigm of hydrogen bonding, that between a pair of water molecules. Using the same computational procedure of M06-2X/6-31+G**, and again correcting for basis set superposition error, the binding energy of the water dimer is computed to be 5.8 kcal/mol. In other words, even without allowing the phenyl ring to interact with the cation, the CH···O hydrogen bonds to the phenol O (7−9 kcal/mol) are considerably stronger than the OH···O hydrogen bond holding two water molecules together. The cation binds even more impressively with the peptide oxygen of NMA; its CH···O hydrogen bonds together produce a binding energy triple that of the water dimer. The enhanced strength of the binding to the cation should not be surprising, since it has been understood for some time that ionic hydrogen bonds are considerably stronger than their neutral counterparts. Taking CH···O hydrogen bonds as a particular example, in the case of neutral dimers, such hydrogen bonds can be small, as in the case of $CH_2FH···OH_2$ where it is perhaps 1.3 kcal/mol[69] or 2.5 kcal/mol for $CHF_2H···OH_2$. In protein-type systems, the binding energy of the $C^{\alpha}H$ of various amino acids lies in the range of 1.9−2.5 kcal/mol,[70] and a similar value is estimated for each CH···O hydrogen bond between the strands of a β-sheet;[71] however, there is clear evidence that placing a charge on either subunit significantly enhances the binding energy to the extent that values exceeding 10 kcal/mol are not unusual.[72−75]

Functional Importance of CH···O Hydrogen Bonds in a Model Methyltransferase. Given the prevalence and strength of CH···O hydrogen bonds, we sought to understand the relative importance of the hydrogen bonding to methyltransferase function. To assess the significance of these interactions, we selected human SET7/9, a protein lysine methyltransferase, as a model system. SET7/9 displays two highly conserved AdoMet methyl CH···O hydrogen bonds that are conserved in the SET domain methyltransferase class.[8,14] One of the hydrogen-bond acceptors is the backbone carbonyl oxygen atom of His-293, whereas the second acceptor is the hydroxyl group of Tyr-335, the invariant tyrosine in the active site of SET domain enzymes (Figure 1E). The tyrosine hydroxyl group accepts a plethora of CH···O hydrogen bonds from the AdoMet methyl group, methylene groups, and adenine C8 atom, in addition to donating a conventional hydrogen bond to a carbonyl group of Ala-295 in the enzyme active site (Figure 4A). Previous studies of SET domain methyltransferases illustrated that the invariant tyrosine is critical to enzyme function,[25,76] but its roles in catalysis and AdoMet recognition remain unresolved. To investigate the functional relevance of the Tyr-335-mediated CH···O hydrogen bonds, we disrupted these interactions by mutating this residue to a phenylalanine.

Before characterizing the effects of the Y335F mutant, we first performed a series of experiments to assess the feasibility of using this mutant to probe AdoMet CH···O hydrogen bonding by examining its stability, ability to bind protein substrate, and maintenance of native structure. Isothermal calorimetry experiments on WT SET7/9 and SET7/9 Y335F demonstrated nearly identical binding affinity for a TAF10 peptide substrate (Figure 5A, Table 1). Thermal denaturation studies illustrated that the Y335F mutant was only modestly destabilized, consistent with the loss of the hydrogen bond between the Tyr-335 hydroxyl group and the carbonyl group of Ala-295 (Figures 4A and 5B). To further examine the effects of the mutation on the enzyme's overall and active site structure, we determined its cocrystal structures in complex with AdoHcy and a TAF10 peptide substrate[26] (Figure 4B−D and Table S2). The coordinates of the Y335F complex and the analogous WT complex superimpose with a Cα RMSD of 0.22 Å, illustrating a high degree of structural similarity between the WT enzyme and the mutant. In comparing the two structures, all conventional hydrogen bonds outside of those between the enzyme and its ligands, AdoHcy and the TAF10 peptide, appear to be preserved as well as the conformations and positions of the active site residues. As prior work demonstrated that the AdoMet methyl ^{1}H chemical shift is highly dependent on its hydrogen-bonding state, we analyzed the AdoMet methyl ^{1}H chemical shift change when bound in the SET7/9 Y335F active site[8] (Figure 5C). Measurement of the AdoMet methyl ^{1}H chemical shift while bound to the Y335F mutant yielded a small upfield chemical shift change (0.1 ppm) relative to the ^{1}H chemical shift measured for the

dx.doi.org/10.1021/ja407140k | J. Am. Chem. Soc. 2013, 135, 15536−15548

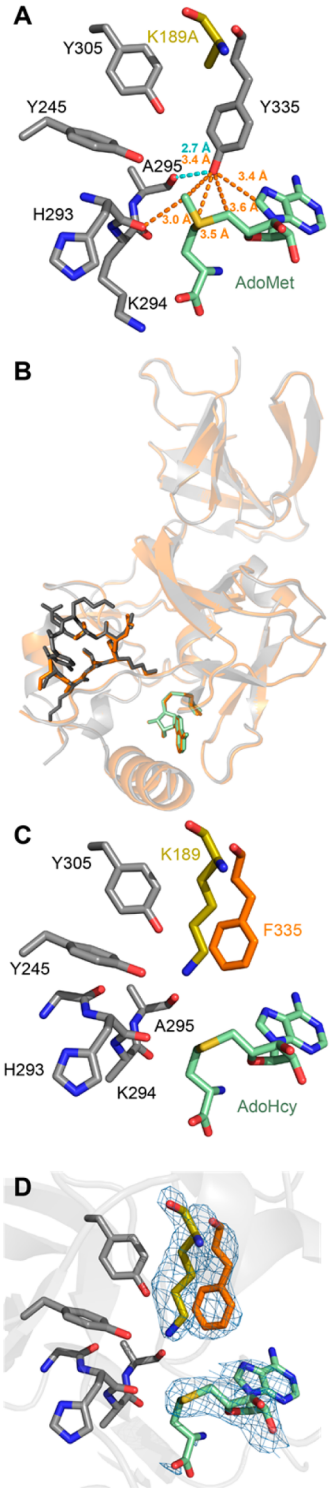

Figure 4. Structure of the WT SET7/9 and Y335F mutant bound to cofactor and the TAF10 peptide. (A) WT SET7/9 (gray carbon atoms) bound to AdoMet (green carbons) and TAF10 K189A peptide (yellow carbons). CH···O and OH···O hydrogen bonds are depicted by orange and cyan dashes with associated distances, respectively. (B) Overlay of WT SET7/9 (3M53, gray)[26] and SET7/9 Y335F (orange), with Cα RMSD = 0.22 Å. AdoHcy and TAF10 peptide are rendered as sticks. (C) Active site of SET7/9 Y335F. (D) $F_o - F_c$ simulated annealing map contoured at 2.0σ for TAF10 K189, AdoHcy, and Phe-335 in the SET7/9 Y335F crystal structure.

WT enzyme, consistent with the loss of the longer CH···O hydrogen bond between the AdoMet methyl and Tyr-335 hydroxyl groups (Figure 4A and 5C). Together, these results emphasize that the SET7/9 Y335F mutant retains the native structure and protein substrate binding properties of the WT enzyme while abolishing the CH···O hydrogen bonds between Tyr-335 and AdoMet, thus validating its use in detailed structure–function comparisons to WT SET7/9.

We next examined whether the Y335F mutant displayed impaired AdoMet binding using a tryptophan fluorescence assay that presumably monitors Trp352, which stacks adjacent to the cofactor adenine group in the enzyme's AdoMet binding pocket. The Y335F mutant diminished AdoMet binding affinity by 3 orders of magnitude, demonstrating that the Tyr-335-mediated CH···O hydrogen bonding is essential for tight binding of the cofactor (Figure 6A, Table 1). Further, the substantial loss of AdoMet binding affinity is consistent with the quantum calculations illustrating that the network of CH···O hydrogen bonds between Tyr-335 and AdoMet is highly stabilizing. We also measured the dissociation constant of the product AdoHcy and mutant and found that the binding affinity is modestly decreased compared to WT (Figure 6), possibly due to the loss of the methylene and adenine C8 hydrogen bonds (Figure 4).

To evaluate the change in catalytic rate of the Y335F mutant, we measured its catalytic turnover as a function of AdoMet concentration using a radiometric methyltransferase assay. Unlike the substantial change observed for the binding compared with WT, the change in catalytic turnover was quite small (Table 1). The Y335F mutant exhibited a k_{cat} value within <2-fold of WT SET7/9 (Figure 7A,B). Single turnover experiments demonstrated that methyl transfer is at least partially rate limiting in SET7/9 (Figure 7C). Although the substantially impaired AdoMet-binding affinity of the Y335F mutant precluded single turnover assays, the similarities in the other biochemical properties of the WT enzyme and the Y335F mutant (e.g., k_{cat} values and AdoHcy and TAF10 peptide dissociation constants (Table 1) and active site structure (Figure 4)) suggest that the rate of methyl transfer was virtually unchanged due to the loss of Tyr-335-mediated CH···O hydrogen bonding. The comparable turnover numbers imply that the CH···O hydrogen bonds contribute a similar level of stabilization to the transition state as to the reactant state in the active site. Thus, the Tyr-335-mediated CH···O hydrogen bonds promote tight binding to AdoMet as well as the transition state but do not differentially recognize these different states. As such, the CH···O hydrogen bonds formed by Tyr-335 in SET7/9 do not appear to promote catalysis via selective transition-state stabilization, instead providing a similar level of stabilization to the transition state as to the reactant state.

Restriction of AdoMet Methyl Motion. Although the Y335F mutation does not appear to alter the methyl transfer rate of SET7/9, this mutation presumably preserves the CH···O hydrogen bond between the AdoMet methyl group and the carbonyl group of His-293. Based upon the NMA modeling results (Figure 3), the His-293 carbonyl group forms a strong hydrogen bond to the AdoMet methyl group that would most likely be the dominant contributor to methyl group positioning and NAC formation.

When bound to SET7/9, the AdoMet methyl group resides in an oxygen-lined aperture, termed the methyl transfer pore, which is composed of the aforementioned hydrogen-bond

dx.doi.org/10.1021/ja407140k | J. Am. Chem. Soc. 2013, 135, 15536–15548

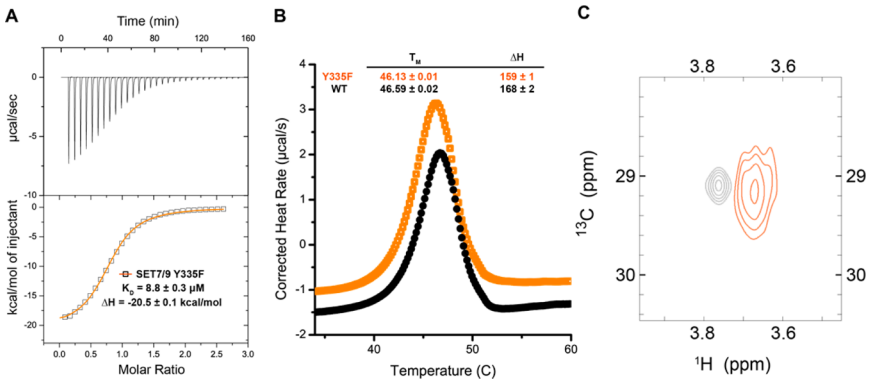

Figure 5. Feasibility tests of the SET7/9 Y335F mutant. (A) ITC analysis of TAF10 binding to SET7/9 Y335F (□). Top panel represents titration of peptide into SET7/9 Y335F, and bottom panel represents binding isotherm with fitted curve. Previous experiments measured a dissociation constant of 4.9 ± 0.1 μM for WT SET7/9 and the TAF10 peptide (Table 1).[26] (B) Differential scanning calorimetry melting of SET7/9 Y335F (□) and WT SET7/9 (●). For clarity, 10 points were omitted between each point shown. (C) WT SET7/9·AdoMet and SET7/9 Y335F·AdoMet methyl ^{1}H chemical shift measurement. WT[8] (gray) and Y335F mutant (orange) ^{13}C 2D-HSQC spectra are overlaid. The Y335F mutation, which removes only the longer methyl CH···O hydrogen bond, causes a small upfield ^{1}H chemical shift change relative to WT SET7/9. The increased line width and lower signal-to-noise of the AdoMet methyl resonance when bound to the Y335F mutant is likely due to lower stability of the Y335F mutant precluding long time course experiments and decreased AdoMet concentration to enable saturation by SET7/9 Y335F.

Table 1. Dissociation Constants and Kinetic Parameters of WT SET7/9 and the Y335F Mutant[a]

	K_D (μM)	
	WT	Y335F
AdoMet	0.053 ± 0.003[b]	52 ± 26[c]
AdoHcy	134 ± 36[c]	714 ± 197[c]
TAF10 peptide	4.9 ± 0.1[b]	8.8 ± 0.3[d]
	kinetic parameters	
	WT	Y335F
k_{cat} (min^{-1})	29.6 ± 0.9	45.2 ± 3.6
k_{cat}/K_M (μM^{-1} min^{-1})	12.0 ± 1.5	0.31 ± 0.068

[a]Kinetic values reported were measured by varying AdoMet concentration and using a fixed saturating concentration of TAF10 peptide. [b]Isothermal titration calorimetry (ITC) values taken from Horowitz et al.[8] and Del Rizzo et al.,[26] respectively. [c]Dissociation constants measured by intrinsic tryptophan fluorescence assay. [d]Dissociation constants measured by ITC.

acceptors and the Gly-264 carbonyl group. To investigate whether CH···O hydrogen bonds may contribute to NAC formation by restricting methyl group motion while bound to the active site, we examined how the geometry of the aperture of the methyl transfer pore changes as a function of the ligands bound in various SET7/9 binary and ternary complexes. To examine these changes, we determined two additional structures of WT SET7/9 ternary complexes bound to a nonreactive peptide (TAF10K189A) and either AdoMet or the product, AdoHcy, to allow comparison of methyl pore size defined by the triangular area of the oxygen atoms of the Gly-264 and His-293 carbonyl groups and the Tyr-335 hydroxyl group (Figure 8). All resulting crystals maintained the same space group with similar unit cell parameters (Table S2) as previous SET7/9·TAF10 peptide ternary complexes[26,44] and diffracted to at least 1.7 Å resolution. Based on the SET7/9 structures analyzed, there is a modest ~15% change in the area of the methyl transfer pore (Figure 8A). The largest and smallest pore areas were observed in the SET7/9·AdoMet binary complex and SET7/9·AdoHcy·TAF10 peptide complex, respectively, which is presumably due to the opposing contributions of the peptide substrate that induces active-site closure in the ternary complex versus the AdoMet methyl group that braces the pore in a more open state. The SET7/9·AdoHcy·TAF10 Kl89A and SET7/9·AdoMet·TAF10 Kl89A peptide complexes exhibit pore areas with intermediate sizes (Figure 8B–D), consistent with slightly reduced active-site closure due to the loss of Lys189 side chain interactions with the enzyme. A plausible explanation for the slightly larger pore

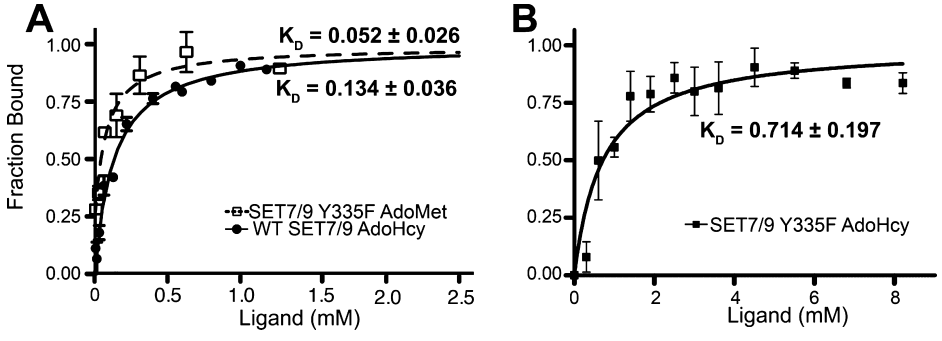

Figure 6. Measurement of cofactor binding affinity by intrinsic tryptophan fluorescence. (A) Binding of AdoHcy to WT SET7/9 (●, solid line) and AdoMet to SET7/9 Y335F (□, dashed line). (B) Binding of AdoHcy to SET7/9 Y335F (■, solid line). All dissociation constants are reported in mM. WT SET7/9 and AdoMet dissociation constant previously measured as 0.053 ± 0.03 μM by ITC (Table 1).[8]

dx.doi.org/10.1021/ja407140k | J. Am. Chem. Soc. 2013, 135, 15536–15548

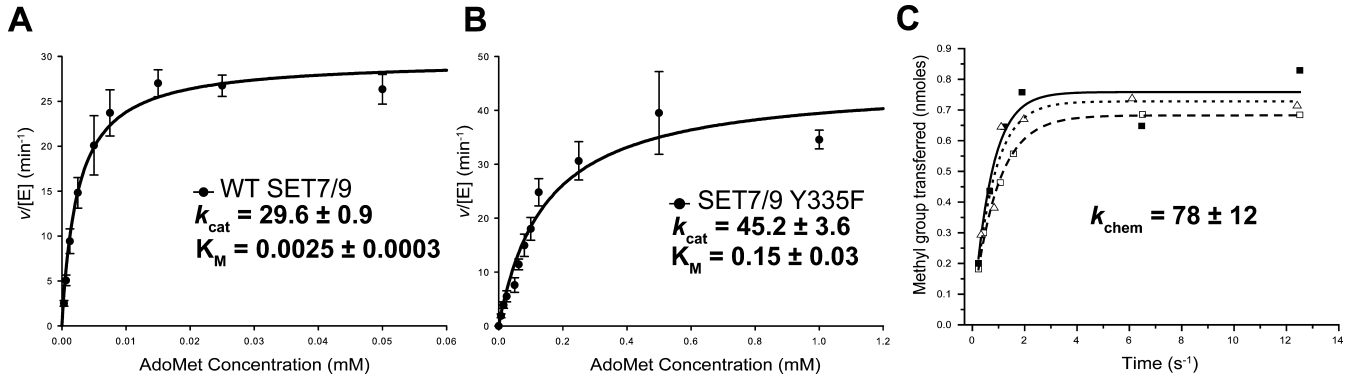

Figure 7. Radiometric methyltransferase assays. Multiple turnover assays with varying AdoMet concentration and a fixed saturating concentration of the TAF10 peptide. Data points and Michaelis–Menten fits are shown for (A) WT SET7/9 and (B) SET7/9Y335F. All k_{cat} values are listed in min^{-1}, and AdoMet K_M values are reported in mM. (C) WT SET7/9 triplicate single turnover experiments SET7/9 at 37 °C. Average parameters from three separate fits: k_{chem} = 1.3 ± 0.2 s^{-1} (78 ± 12 min^{-1}) maximum product produced = 0.72 ± 0.04 nmoles. Open triangles and dotted line represent 140 μM enzyme concentration. Open and solid squares represent 70 μM enzyme assays.

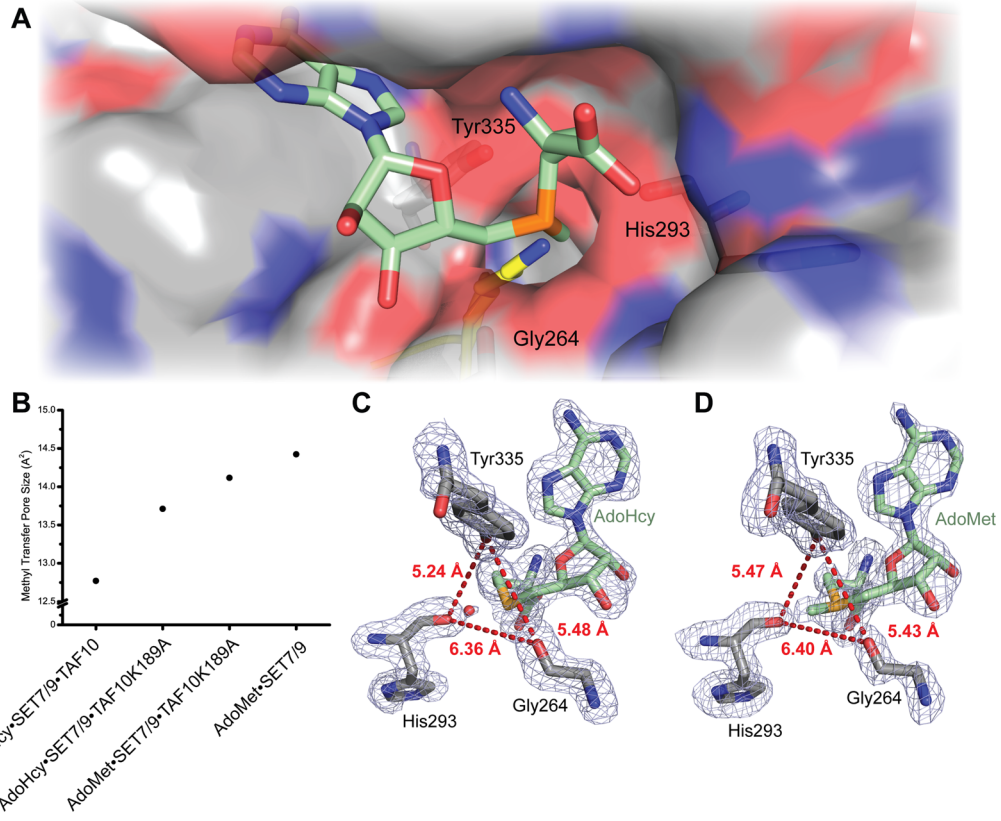

Figure 8. Methyl transfer pore of SET7/9. (A) View of oxygen-lined methyl transfer pore in SET7/9. AdoMet and lysine are rendered with green and yellow carbon atoms, respectively. The SET7/9 surface is illustrated using CPK coloring. The model was created using SET7/9·TAF10 K189A·AdoMet structure superimposed upon the SET7/9·TAF10·AdoHcy structure[26] (PDB accession code 3M53). (B) Methyl transfer pore increases as a function of active site substituent. The size of the pore is defined as the area of the triangle formed by the carbonyl oxygen atoms of His-293 and Gly264 and the hydroxyl group of Tyr-335. PDB accession codes for the other SET7/9 complexes besides those reported here are, in order of appearance: 3M53[26] and 1N6A.[29] (C, D) Simulated annealing omit maps (contoured at 2.5σ) and methyl transfer pore sizes for crystal structures of SET7/9·TAF10 K189A·AdoHcy and SET7/9·TAF10 K189A·AdoMet, respectively, with the methyl transfer pore triangle shown in red dashes.

area of the AdoMet complexes is consistent with the introduction of the AdoMet methyl group's steric footprint within the pore. Together, these structures led us to hypothesize that the size of the methyl transfer pore may constrain the AdoMet methyl group's amplitude of motion, potentially favoring NAC formation during catalysis.

To directly probe this question, we analyzed the motion of the AdoMet S–C_{methyl} bond axis using the generalized order parameter (S^2_{axis}). This parameter specifically measures the amplitude of motion of the S–C axis on a scale of 0 to 1 and is insensitive to rotational methyl motion as well as motions parallel to the S–C axis. Importantly, S^2_{axis} can both be back-calculated from structural ensembles as well as derived using Model-Free analysis and NMR spin-relaxation experiments. For a point of reference for our analysis, the average alanine methyl S^2_{axis} in proteins, which shares some stereochemical similarity to

dx.doi.org/10.1021/ja407140k | J. Am. Chem. Soc. 2013, 135, 15536–15548

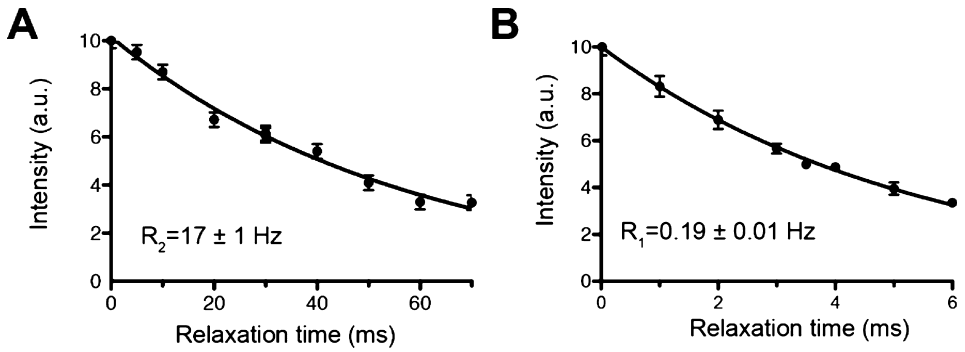

Figure 9. NMR dynamics analysis of AdoMet bound to SET7/9. (A) R_2 and (B) R_1 ^{13}C spin relaxation fits of $^{13}CHD_2$-methyl AdoMet bound to SET7/9.

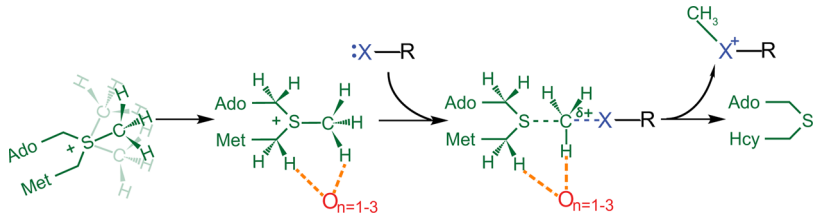

Figure 10. Model of AdoMet-dependent methylation. CH···O hydrogen-bond formation restricts methyl movement and stabilizes both the reactant and sp^2 transition states.

AdoMet due to its relatively fixed sp^3 Cα atom, was previously shown to be 0.8.[77] To evaluate the extent of motion of the AdoMet methyl group when not bound to the methyltransferase active site, we calculated the S^2_{axis} for the free AdoMet using an MD simulation previously verified to accurately reflect the level of AdoMet methyl CH···O hydrogen bonding in water[8] and found the S^2_{axis} = 0.67. To compare the methyltransferase-bound S^2_{axis} with the free AdoMet, we calculated S^2_{axis} from the methyltransferase crystal structures used in the PDB survey (S^2_{axis} = 0.96) (Table S1), demonstrating that the AdoMet methyl group is fixed in position to a greater degree than for free AdoMet in solution or for the analogous alanine methyl groups. Finally, to confirm this observation, we directly measured the AdoMet methyl motion while bound to WT SET7/9 in solution by NMR ^{13}C spin-relaxation experiments (Figure 9). Using the Model-Free formalism,[41] the AdoMet methyl group was observed to have an order parameter (S^2_{axis}) of 1.2 ± 0.2, confirming that the S−C bond axis of the methyl group experiences little to no motion when bound in the active site, and substantially less motion than when free in solution. Although the AdoMet methyl S^2_{axis} could not be measured in the Y335F mutant (Figure 5C), these results indicate that the methyl transfer pore restricts the motion of the AdoMet methyl group in the active site, presumably optimizing catalytic alignment and favoring NAC formation.

DISCUSSION

The results presented here illustrate that methyl CH···O hydrogen bonds are a highly conserved and important contributor to AdoMet-dependent methylation. In SET7/9, the CH···O hydrogen bonds formed by the Tyr-335 hydroxyl group (Figure 4A) are essential for high-affinity AdoMet binding and transition-state stabilization. Quantum chemistry calculations of an AdoMet mimic forming CH···O hydrogen bonds with phenol and NMA illustrate the relative strength of these interactions as compared to other types of CH···O hydrogen bonds, due to the charged nature of the interaction (Figure 3). Further, the methyl transfer pore formed by CH···O hydrogen-bond acceptors in the active site of SET7/9 (Figure 8) is responsible for limiting the motion of the AdoMet methyl group (Figure 9), potentially contributing to NAC formation. Together, the methyltransferase structural survey, computational, biochemical, crystallographic, and NMR dynamics results point toward a convergent evolutionary model for AdoMet-dependent methylation that is contingent upon CH···O hydrogen bonding (Figure 10). Future studies will be needed to examine the potential contributions of AdoMet CH···O hydrogen bonding in catalysis, particularly with respect to electrostatics, compression, and NAC formation.

In addition to Tyr-335, the carbonyl group of His-293 engages in a CH···O hydrogen bond to the AdoMet methyl group with an interaction distance shorter than that of the Tyr-335 hydroxyl group (Figure 4A). Although the function of this carbonyl group cannot be readily probed by site-directed mutagenesis, the analysis of the methyl transfer pore and NMR dynamics as well as the QM calculations provides potential insights into the functions of the His-293 carbonyl-AdoMet methyl CH···O hydrogen bond through promoting binding, transition-state stabilization, and potentially NAC formation. Notably, the QM calculations suggest that this carbonyl group engages in substantially stronger CH···O hydrogen bonding to AdoMet than the tyrosine side chain (Figure 3). This carbonyl-methyl CH···O hydrogen bond is highly conserved in the active sites of SET domain methyltransferases (Table S1) with short interaction distances comparable to that observed in SET7/9 (Figure 4A), consistent with the prediction of strong CH···O hydrogen bonding. Indeed, the structural survey found that in all methyltransferases, carbonyl groups constituted the largest category (52%) of AdoMet methyl CH···O hydrogen-bond acceptors (Table S1). These carbonyl-mediated hydrogen bonds may have functions that differ from those formed with residues bearing hydroxyl groups with respect to binding and catalysis. Further studies are needed to define the functions of carbonyl-methyl CH···O hydrogen bonding in AdoMet binding

dx.doi.org/10.1021/ja407140k | J. Am. Chem. Soc. 2013, 135, 15536−15548

and catalysis in the different methyltransferase classes. Other lines of evidence for the functions of CH···O hydrogen bonds in methyltransferases that merit further investigation include the reported CD_3-AdoMet deuterium isotope effects measured in catechol-*O*-methyltransferase (COMT)[78] and cyclopropane fatty acid synthase[79] as well as AdoMet analogs utilized for identifying new methyltransferase substrates that may alter the reactivity of the electrophile.[80,81]

AdoMet-dependent methyltransferases are emerging as a broad class of therapeutic targets for treating cancer,[82−84] HIV,[85] bacterial infections,[86] malaria,[87] and neurological disorders.[88] Knowledge of the importance and prevalence of AdoMet CH···O hydrogen bonding can be exploited in structure-based design of small molecule inhibitors for methyltransferases employing at least two distinct strategies: (1) targeting the methyltransferase·AdoMet complex using ligands with functional groups that act as CH···O hydrogen-bond acceptors to AdoMet or (2) mimicking the AdoMet CH···O hydrogen-bond donors using cofactor or transition-state analogs. The first strategy is exemplified by tolcapone, an inhibitor of COMT that is used in adjunctive therapy for Parkinson's disease.[88] The crystal structure of the COMT·AdoMet·Tolcapone complex[89] illustrates a short CH···O hydrogen bond (3.0 Å) between the AdoMet methyl group and the drug's nitro substituent, similar to CH···O hydrogen bonds formed between the AdoMet and the enzyme, which presumably enhances the drug's binding affinity. With respect to the second strategy, Luo and co-workers have recently introduced a new class of transition-state or bisubstrate analog methyltransferase inhibitors by derivatizing sinefungin, a natural product AdoMet analog that inhibits a wide array of methyltransferases.[90] Sinefungin differs from AdoMet in that the methyl-sulfonium cation is substituted by an amine-methylene group that is capable of forming conventional NH···O hydrogen bonds in place of the methyl CH···O hydrogen bonds with the same hydrogen-bond acceptors in the active site.[14] The feasibility of using sinefungin as a scaffold for designing selective and potent inhibitors was recently demonstrated with the SET domain methyltransferase SETD2.[90] Together, we envision that these strategies will offer fortuitous avenues for developing new classes of methyltransferase inhibitors to treat numerous diseases.

Given the widespread occurrence of CH···O hydrogen bonds in biology[11] and their crucial importance in the particular case described in this article, it is important to accurately represent these interactions in empirical force fields. Presently, many force fields lack explicit hydrogen-bond potentials, instead relying upon implicit electrostatics. In contrast, crystal structure refinement programs do not commonly include electrostatic terms. Due to this omission, it seems probable that refinements of crystal structures that are based upon such algorithms will result in structures with C···O distances that are too long and CH···O hydrogen-bond angles that are too acute, particularly in lower-resolution structures or in situations involving strong ionic CH···O hydrogen bonds, such as observed for AdoMet. Consequently, biological structures refined by potentials that do not properly reflect CH···O attractions may mistakenly under-report CH···O hydrogen bonding. In addition, proper parametrization of small molecules for computational inhibitor design may also benefit from a better understanding of strong CH···O hydrogen bonding, particularly in the development of AdoMet-based methyltransferase inhibitors.

CONCLUSIONS

The biochemical and computational data presented here implicate CH···O hydrogen bonding as an important contributor to AdoMet binding and methyl transfer. QM calculations of AdoMet CH···O hydrogen bond strengths illustrate the strengths of these interactions, which exceed that of typical CH···O hydrogen bonds. In addition, analysis of the methyl transfer pore dynamics by X-ray crystallography and NMR spectroscopy suggests that the CH···O hydrogen bonds may contribute to catalysis by promoting NAC formation. An understanding of these hydrogen bonds in the active sites of different methyltransferases can be leveraged in designing new, more potent methyltransferases inhibitors.

ASSOCIATED CONTENT

Supporting Information

Supporting Information contains Figures S1 and S2 and Tables S1 and S2. This information is available free of charge via the Internet at http://pubs.acs.org.

AUTHOR INFORMATION

Corresponding Author

rtrievel@umich.edu

Notes

The authors declare no competing financial interest.

ACKNOWLEDGMENTS

The authors would like to thank S. Bulfer and P. Del Rizzo for aid in the methyltransferase survey, A. Hansen, L. Salmon, and J. Chugh for aid in NMR experiments and interpretation, and R. Ishima and V. Tugarinov for providing published pulse sequences. The authors would also like to thank T. Cierpicki, R. Banerjee, C. Thorpe, A. Karplus, and P. O'Brien for reading and commenting on the manuscript. Use of the Advanced Photon Source was supported by the U.S. Department of Energy, under contract no. DE-AC02-06CH11357. Computer, storage, and other resources from the Division of Research Computing in the Office of Research and Graduate Studies at Utah State University are gratefully acknowledged. This work was supported by NSF-MCB-0448297 to R.A.M., by grants from the University of Michigan's Biomedical Research Council and the Office for the Vice President for Research and NSF (CHE-1213484) to R.C.T., the Kentucky Agriculture Experiment station Hatch project no. KY011031 to R.L.H., and NSF-CHE-1026826 to S.S. Use of the LS-CAT Sector 21 was supported by the Michigan Economic Development Corporation and the Michigan Technology Tri-Corridor (grant 085P1000817).

REFERENCES

(1) Schubert, H. L.; Blumenthal, R. M.; Cheng, X. D. *Trends Biochem. Sci.* **2003**, *28*, 329.
(2) Fontecave, M.; Atta, M.; Mulliez, E. *Trends Biochem. Sci.* **2004**, *29*, 243.
(3) Petrossian, T. C.; Clarke, S. G. *Mol. Cell. Proteomics* **2011**, *10*, M110.000976.
(4) Grove, T. L.; Benner, J. S.; Radle, M. I.; Ahlum, J. H.; Landgraf, B. J.; Krebs, C.; Booker, S. J. *Science* **2011**, *332*, 604.
(5) Lau, E. Y.; Bruice, T. C. *J. Am. Chem. Soc.* **1998**, *120*, 12387.
(6) Zhang, J. Y.; Klinman, J. P. *J. Am. Chem. Soc.* **2011**, *133*, 17134.
(7) Soriano, A.; Castillo, R.; Christov, C.; Andres, J.; Moliner, V.; Tunon, I. *Biochemistry* **2006**, *45*, 14917.
(8) Horowitz, S.; Yesselman, J. D.; Al-Hashimi, H. M.; Trievel, R. C. *J. Biol. Chem.* **2011**, *286*, 18658.

(9) Arbely, E.; Arkin, I. T. *J. Am. Chem. Soc.* **2004**, *126*, 5362.
(10) Scheiner, S. *Phys. Chem. Chem. Phys.* **2011**, *13*, 13860.
(11) Horowitz, S.; Trievel, R. C. *J. Biol. Chem.* **2012**, *287*, 41576.
(12) Derewenda, Z. S.; Lee, L.; Derewenda, U. *J. Mol. Biol.* **1995**, *252*, 248.
(13) Jiang, L.; Lai, L. H. *J. Biol. Chem.* **2002**, *277*, 37732.
(14) Couture, J. F.; Hauk, G.; Thompson, M. J.; Blackburn, G. M.; Trievel, R. C. *J. Biol. Chem.* **2006**, *281*, 19280.
(15) Ash, E. L.; Sudmeier, J. L.; Day, R. M.; Vincent, M.; Torchilin, E. V.; Haddad, K. C.; Bradshaw, E. M.; Sanford, D. G.; Bachovchin, W. W. *Proc. Natl. Acad. Sci. U.S.A.* **2000**, *97*, 10371.
(16) Klaholz, B. P.; Moras, D. *Structure* **2002**, *10*, 1197.
(17) Kleywegt, G. J.; Harris, M. R.; Zou, J. Y.; Taylor, T. C.; Wahlby, A.; Jones, T. A. *Acta Crystallogr., Sect. D: Biol. Crystallogr.* **2004**, *60*, 2240.
(18) Emsley, P.; Lohkamp, B.; Scott, W. G.; Cowtan, K. *Acta Crystallogr., Sect. D: Biol. Crystallogr.* **2010**, *66*, 486.
(19) Vargas, R.; Garza, J.; Dixon, D. A.; Hay, B. P. *J. Am. Chem. Soc.* **2000**, *122*, 4750.
(20) Yesselman, J. D.; Price, D. J.; Knight, J. L.; Brooks, C. L., III *J. Comput. Chem.* **2012**, *33*, 189−202.
(21) Steiner, T. *J. Phys. Chem. A* **2000**, *104*, 433.
(22) Pierce, A. C.; Sandretto, K. L.; Bemis, G. W. *Proteins: Struct., Funct., Genet.* **2002**, *49*, 567.
(23) Fisher, R. a.; Yates, F. *Statistical Tables for Biological, Agricultural, and Medical Research*, 3rd ed.; Oliver & Boyd: London, 1948.
(24) Pettersen, E. F.; Goddard, T. D.; Huang, C. C.; Couch, G. S.; Greenblatt, D. M.; Meng, E. C.; Ferrin, T. E. *J. Comput. Chem.* **2004**, *25*, 1605.
(25) Trievel, R. C.; Beach, B. M.; Dirk, L. M. A.; Houtz, R. L.; Hurley, J. H. *Cell* **2002**, *111*, 91.
(26) Del Rizzo, P. A.; Couture, J. F.; Dirk, L. M. A.; Strunk, B. S.; Roiko, M. S.; Brunzelle, J. S.; Houtz, R. L.; Trievel, R. C. *J. Biol. Chem.* **2010**, *285*, 31849.
(27) Otwinowski, Z.; Minor, W. *Methods Enzymol.* **1997**, *276*, 307.
(28) Vagin, A.; Teplyakov, A. *Acta Crystallogr., Sect. D: Biol. Crystallogr.* **2000**, *56*, 1622.
(29) Kwon, T.; Chang, J. H.; Kwak, E.; Lee, C. W.; Joachimiak, A.; Kim, Y. C.; Lee, J. W.; Cho, Y. J. *EMBO J.* **2003**, *22*, 292.
(30) Vagin, A. A.; Steiner, R. A.; Lebedev, A. A.; Potterton, L.; McNicholas, S.; Long, F.; Murshudov, G. N. *Acta Crystallogr., Sect. D: Biol. Crystallogr.* **2004**, *60*, 2184.
(31) Chen, V. B.; Arendall, W. B.; Headd, J. J.; Keedy, D. A.; Immormino, R. M.; Kapral, G. J.; Murray, L. W.; Richardson, J. S.; Richardson, D. C. *Acta Crystallogr., Sect. D: Biol. Crystallogr.* **2010**, *66*, 12.
(32) Brunger, A. T.; Adams, P. D.; Clore, G. M.; DeLano, W. L.; Gros, P.; Grosse-Kunstleve, R. W.; Jiang, J. S.; Kuszewski, J.; Nilges, M.; Pannu, N. S.; Read, R. J.; Rice, L. M.; Simonson, T.; Warren, G. L. *Acta Crystallogr., Sect. D: Biol. Crystallogr.* **1998**, *54*, 905.
(33) Delaglio, F.; Grzesiek, S.; Vuister, G. W.; Zhu, G.; Pfeifer, J.; Bax, A. *J. Biomol. NMR* **1995**, *6*, 277.
(34) Goddard, T. G., Kneller, D. G. *SPARKY 3*; University of California: San Francisco, CA.
(35) Hansen, A. L.; Al-Hashimi, H. M. *J. Am. Chem. Soc.* **2007**, *129*, 16072.
(36) Hansen, A. L.; Nikolova, E. N.; Casiano-Negroni, A.; Al-Hashimi, H. M. *J. Am. Chem. Soc.* **2009**, *131*, 3818.
(37) Ishima, R.; Louis, J. M.; Torchia, D. A. *J. Am. Chem. Soc.* **1999**, *121*, 11589.
(38) Zhang, Q.; Sun, X. Y.; Watt, E. D.; Al-Hashimi, H. M. *Science* **2006**, *311*, 653.
(39) de la Torre, J. G.; Huertas, M. L.; Carrasco, B. *J. Magn. Reson.* **2000**, *147*, 138.
(40) Cho, C. H.; Urquidi, J.; Singh, S.; Robinson, G. W. *J. Phys. Chem. B* **1999**, *103*, 1991.
(41) Ishima, R.; Petkova, A. P.; Louis, J. M.; Torchia, D. A. *J. Am. Chem. Soc.* **2001**, *123*, 6164.
(42) Markwick, P. R. L.; Bouvignies, G.; Blackledge, M. *J. Am. Chem. Soc.* **2007**, *129*, 4724.
(43) Chandrasekhar, I.; Clore, G. M.; Szabo, A.; Gronenborn, A. M.; Brooks, B. R. *J. Mol. Biol.* **1992**, *226*, 239.
(44) Couture, J. F.; Dirk, L. M. A.; Brunzelle, J. S.; Houtz, R. L.; Trievel, R. C. *Proc. Natl. Acad. Sci. U.S.A.* **2008**, *105*, 20659.
(45) Chirpich, T. P.; Zappia, V.; Costilow, R. N.; Barker, H. A. *J. Biol. Chem.* **1970**, *245*, 1778.
(46) Frisch, M. J.; Trucks, G. W.; Schlegel, H. B.; Scuseria, G. E.; Robb, M. A.; Cheeseman, J. R.; Scalmani, G.; Barone, V.; Mennucci, B.; Petersson, G. A.; Nakatsuji, H.; Caricato, M.; Li, X.; Hratchian, H. P.; Izmaylov, A. F.; Bloino, J.; Zheng, G.; Sonnenberg, J. L.; Hada, M.; Ehara, M.; Toyota, K.; Fukuda, R.; Hasegawa, J.; Ishida, M.; Nakajima, T.; Honda, Y.; Kitao, O.; Nakai, H.; Vreven, T.; Montgomery, J. A., Jr.; Peralta, J. E.; Ogliaro, F.; Bearpark, M.; Heyd, J. J.; Brothers, E.; Kudin, K. N.; Staroverov, V. N.; Kobayashi, R.; Normand, J.; Raghavachari, K.; Rendell, A.; Burant, J. C.; Iyengar, S. S.; Tomasi, J.; Cossi, M.; Rega, N.; Millam, J. M.; Klene, M.; Knox, J. E.; Cross, J. B.; Bakken, V.; Adamo, C.; Jaramillo, J.; Gomperts, R.; Stratmann, R. E.; Yazyev, O.; Austin, A. J.; Cammi, R.; Pomelli, C.; Ochterski, J. W.; Martin, R. L.; Morokuma, K.; Zakrzewski, V. G.; Voth, G. A.; Salvador, P.; Dannenberg, J. J.; Dapprich, S.; Daniels, A. D.; Farkas, O.; Foresman, J. B.; Ortiz, J. V.; Cioslowski, J.; Fox, D. J. *Gaussian 09*, revision B.01; Gaussian, Inc.: Wallingford, CT, 2009.
(47) Zhao, Y.; Truhlar, D. G. *J. Phys. Chem. A* **2006**, *110*, 5121.
(48) Hohenstein, E. G.; Chill, S. T.; Sherrill, C. D. *J. Chem. Theory Comput.* **2008**, *4*, 1996.
(49) Biller, M. J.; Mecozzi, S. *Mol. Phys.* **2012**, *110*, 377.
(50) Podeszwa, R.; Szalewicz, K. *J. Chem. Phys.* **2012**, *136*, 161102.
(51) Forni, A.; Pieraccini, S.; Rendine, S.; Gabas, F.; Sironi, M. *ChemPhysChem* **2012**, *13*, 4224.
(52) Kozuch, S.; Martin, J. M. L. *J. Chem. Theory Comput.* **2013**, *9*, 1918.
(53) Kerdawy, A. E.; Murray, J. S.; Politzer, P.; Bleiziffer, P.; Heßelmann, A.; Görling, A.; Clark, T. *J. Chem. Theory Comput.* **2013**, *9*, 2264.
(54) Remya, K.; Suresh, C. H. *J. Comput. Chem.* **2013**, *34*, 1341.
(55) Doemer, M.; Tavernelli, I.; Rothlisberger, U. *J. Chem. Theory Comput.* **2013**, *17*, 955.
(56) Rosokha, S. V.; Stern, C. L.; Ritzert, J. T. *Chem.−Eur. J.* **2013**, *19*, 8774.
(57) Boys, S. F.; Bernardi, F. *Mol. Phys.* **1970**, *19*, 553.
(58) Scheiner, S. *J. Phys. Chem. A* **2011**, *115*, 11202.
(59) Griffith, S. C.; Sawaya, M. R.; Boutz, D. R.; Thapar, N.; Katz, J. E.; Clarke, S.; Yeates, T. O. *J. Mol. Biol.* **2001**, *313*, 1103.
(60) Dixon, M. M.; Huang, S.; Matthews, R. G.; Ludwig, M. *Structure* **1996**, *4*, 1263.
(61) Nureki, O.; Watanabe, K.; Fukai, S.; Ishii, R.; Endo, Y.; Hori, H.; Yokoyama, S. *Structure* **2004**, *12*, 593.
(62) Boal, A. K.; Grove, T. L.; McLaughlin, M. I.; Yennawar, N. H.; Booker, S. J.; Rosenzweig, A. C. *Science* **2011**, *332*, 1089.
(63) Yang, J.; Kulkarni, K.; Manolaridis, I.; Zhang, Z.; Dodd, R. B.; Mas-Droux, C.; Barford, D. *Mol. Cell* **2011**, *44*, 997.
(64) Schubert, H. L.; Wilson, K. S.; Raux, E.; Woodcock, S. C.; Warren, M. J. *Nat. Struct. Biol.* **1998**, *5*, 585.
(65) Suzuki, Y.; Noma, A.; Suzuki, T.; Ishitani, R.; Nureki, O. *Nucleic Acids Res.* **2009**, *37*, 2910.
(66) Gilli, G.; Gilli, P. *The Nature of the Hydrogen Bond*; Oxford University Press: New York, 2009.
(67) Steiner, T.; Desiraju, G. R. *Chem Commun* **1998**, 891.
(68) Adhikari, U.; Scheiner, S. *J. Phys. Chem. A* **2013**, *117*, 489.
(69) Gu, Y.; Kar, T.; Scheiner, S. *J. Am. Chem. Soc.* **1999**, *121*, 9411.
(70) Scheiner, S.; Kar, T.; Gu, Y. *J. Biol. Chem.* **2001**, *276*, 9832.
(71) Scheiner, S. *J. Phys. Chem. B* **2006**, *110*, 18670.
(72) Lee, K.-M.; Chen, J. C. C.; Chen, H.-Y.; Lin, I. J. B. *Chem Commun* **2012**, *48*, 1242.
(73) Ramabhadran, R. O.; Hua, Y.; Li, Y.-j.; Flood, A. H.; Raghavachari, K. *Chem.−Eur. J.* **2011**, *17*, 9123.
(74) Pedzisa, L.; Hay, B. P. *J. Org. Chem.* **2009**, *74*, 2554.

(75) Scheiner, S.; Kar, T.; Pattanayak, J. *J. Am. Chem. Soc.* **2002**, *124*, 13257.
(76) Zhang, X.; Tamaru, H.; Khan, S. I.; Horton, J. R.; Keefe, L. J.; Selker, E. U.; Cheng, X. D. *Cell* **2002**, *111*, 117.
(77) Igumenova, T. I.; Frederick, K. K.; Wand, A. J. *Chem Rev* **2006**, *106*, 1672.
(78) Hegazi, M. F.; Borchardt, R. T.; Schowen, R. L. *J. Am. Chem. Soc.* **1979**, *101*, 4359.
(79) Iwig, D. F.; Grippe, A. T.; McIntyre, T. A.; Booker, S. J. *Biochemistry-Us* **2004**, *43*, 13510.
(80) Islam, K.; Zheng, W.; Yu, H.; Deng, H.; Luo, M. *ACS Chem. Biol.* **2011**, *6*, 679.
(81) Lee, B. W.; Sun, H. G.; Zang, T.; Kim, B. J.; Alfaro, J. F.; Zhou, Z. S. *J. Am. Chem. Soc.* **2010**, *132*, 3642.
(82) Copeland, R. A.; Solomon, M. E.; Richon, V. M. *Nat. Rev. Drug Discovery* **2009**, *8*, 724.
(83) Singh, V.; Sharma, P.; Capalash, N. *Curr. Cancer Drug Targets* **2013**, *13*, 379.
(84) Greer, E. L.; Shi, Y. *Nat. Rev. Genet.* **2012**, *13*, 343.
(85) Pagans, S.; Kauder, S. E.; Kaehlcke, K.; Sakane, N.; Schroeder, S.; Dormeyer, W.; Trievel, R. C.; Verdin, E.; Schnolzer, M.; Ott, M. *Cell Host Microbe* **2010**, *7*, 234.
(86) Grosjean, H. *DNA and RNA modification enzymes: structure, mechanism, function, and evolution*; Landes Bioscience: Austin, TX, 2009.
(87) Lee, S. G.; Kim, Y.; Alpert, T. D.; Nagata, A.; Jez, J. M. *J. Biol. Chem.* **2012**, *287*, 1426.
(88) Mannisto, P. T.; Kaakkola, S. *Pharmacol. Rev.* **1999**, *51*, 593.
(89) Ellermann, M.; Lerner, C.; Burgy, G.; Ehler, A.; Bissantz, C.; Jakob-Roetne, R.; Paulini, R.; Allemann, O.; Tissot, H.; Grunstein, D.; Stihle, M.; Diederich, F.; Rudolph, M. G. *Acta Crystallogr., Sect. D: Biol. Crystallogr.* **2012**, *68*, 253.
(90) Zheng, W.; Ibanez, G.; Wu, H.; Blum, G.; Zeng, H.; Dong, A.; Li, F.; Hajian, T.; Allali-Hassani, A.; Amaya, M. F.; Siarheyeva, A.; Yu, W.; Brown, P. J.; Schapira, M.; Vedadi, M.; Min, J.; Luo, M. *J. Am. Chem. Soc.* **2012**, *134*, 18004.

Conservation and Functional Importance of Carbon-Oxygen Hydrogen Bonding in AdoMet-Dependent Methyltransferases

Scott Horowitz, Lynnette M.A. Dirk, Joseph D. Yesselman, Jennifer S. Nimtz, Upendra Adhikari, Ryan A. Mehl, Steve Scheiner, Robert L. Houtz, Hashim M. Al-Hashimi, Raymond C. Trievel

Supplemental Information

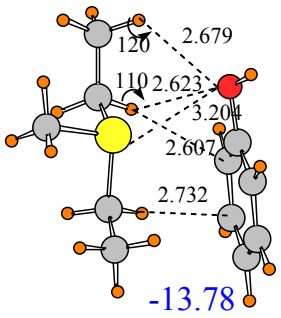

-13.78

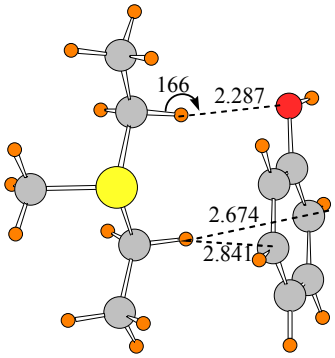

-13.49

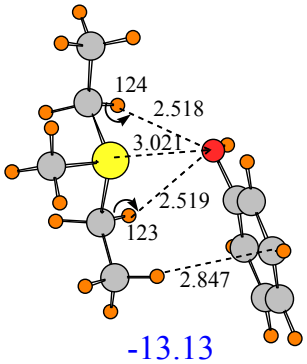

-13.13

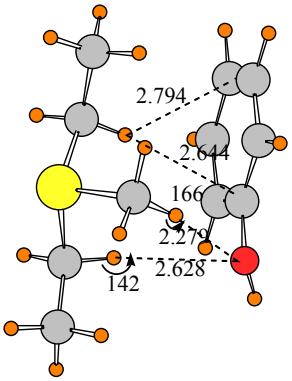

-12.98

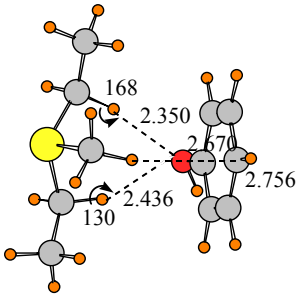

-12.86

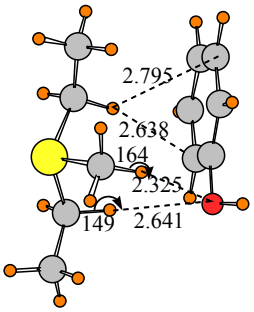

-12.55

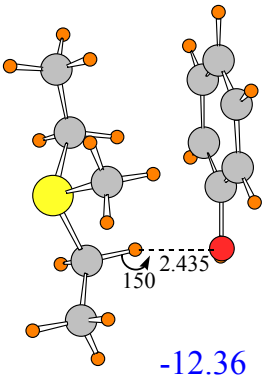

-12.36

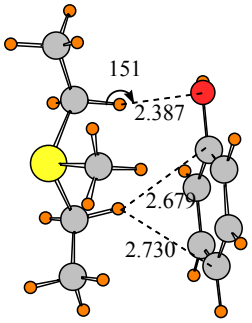

-12.34

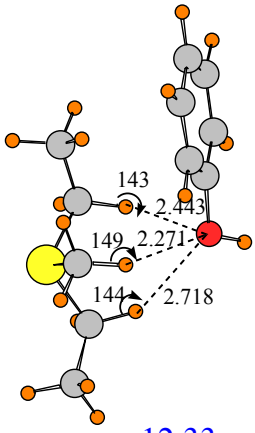

-12.33

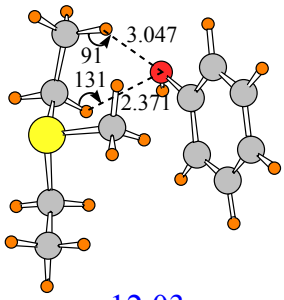

-12.03

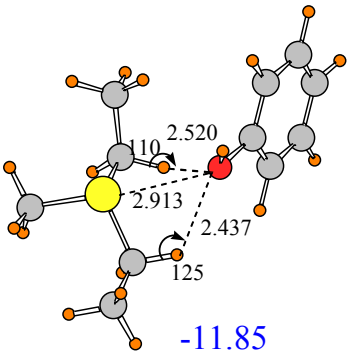

-11.85

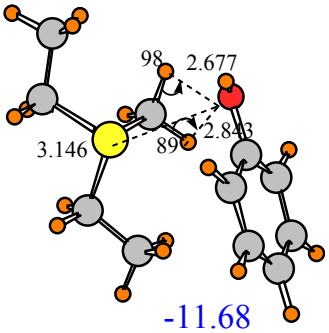

-11.68

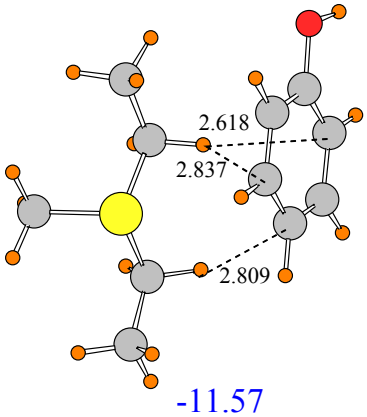

-11.57

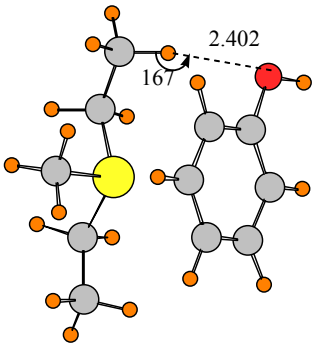

-11.50

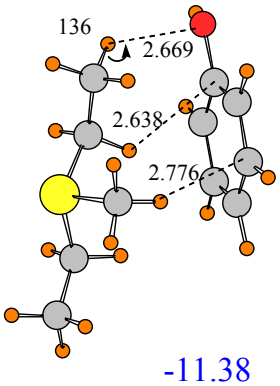

-11.38

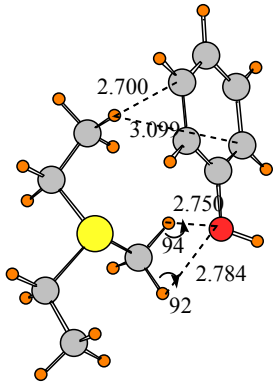

-11.37

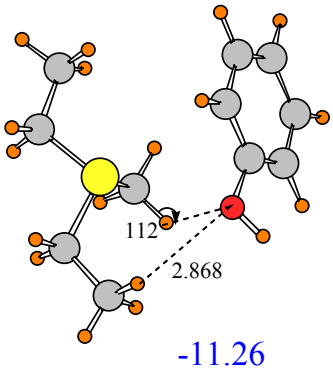

-11.26

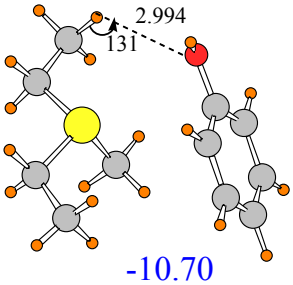

-10.70

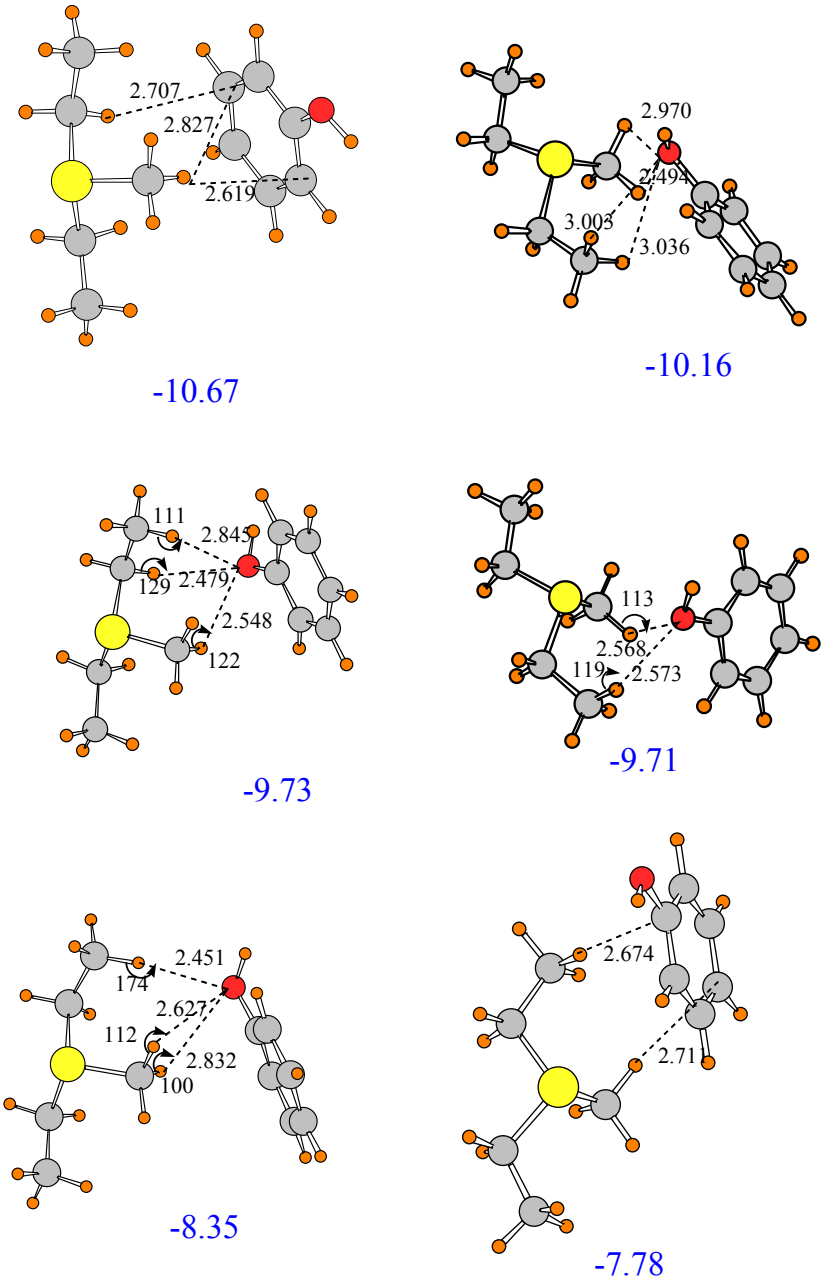

Figure S1: All energies and coordinates of $SMe(Et)_2^+$ cation···phenol minima.

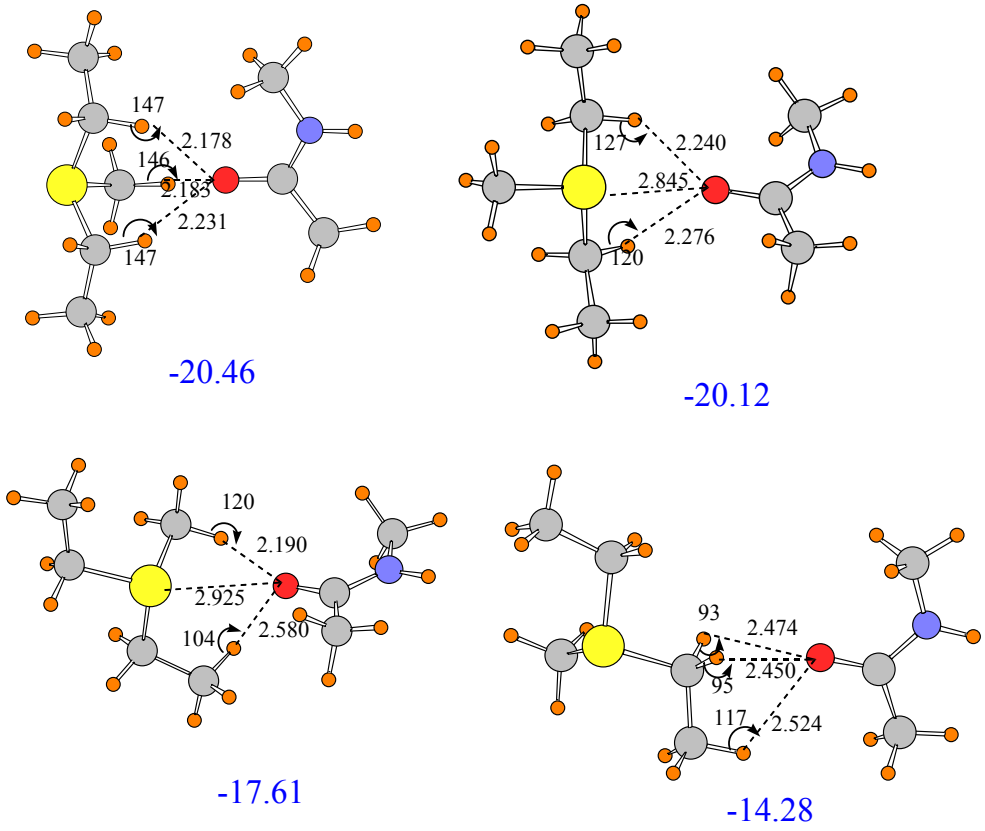

Figure S2: All energies and coordinates of $SMe(Et)_2^+$ cation···N-methylacetamide minima.

PDB	Acceptor Residue	Acceptor Atom	Acceptor Residue Number	C···O distance (Å)
1EIZ	ASP	O	124	3.38
1EIZ	HOH	O	421	3.59
1EJ0	HOH	O	421	3.49
1EJ0	ASP	O	124	3.56
1G60	HOH	O	561/570	3.00
1G60	HOH	O	583	3.00
1JG4	THR	O	73	2.81
1MSK	SAM	O4'	1301	3.02
1MSK	HOH	O	2174	3.50
1N2X	ASP	OD1	103	2.43
1N2X	ASP	O	103	3.16
1N6A	HIS	O	293	3.00
1N6A	TYR	OH	335	3.48
1RJD	HOH	O	905/845	3.49
1RJD	CYS	O	202	3.54
1V2X	GLU	O	124	2.59
1V2X	HOH	O	442	2.96
1ZQ9	HOH	O	4166	3.09
2AVD	SER	O	84	3.27
2AVD	ASP	OD1	185	3.51
2B9E	ASP	O	305	3.44
2CL5	BIE*	O3	1218	3.24
2CL5	ASP	O	141	3.37
2CL5	MET	O	40	3.38
2CL5	HOH	O	2205/2186	3.67
2DPM	ASP	O	194	3.25
2NPN	TYR	O	115	3.08
2NPN	HOH	O	4781	3.08
2NXE	HOH	O	336	2.82
2NYU	ASP	O	104	3.42
2PLW	HOH	O	216	3.22
2WA2	HOH	O	2149	3.46
2ZUL	ASN	O	305	3.15
3AIA	HIS	O	158	3.06
3AIA	ASP	O	157	3.21
3CKK	PHE	O	131	2.90
3DLC	GLY	O	118	3.29
3DMF	ASN	O	305	3.21
3DOU	HOH	O	255	3.61
3DOU	ASP	O	111	3.68

3DXY	PHE	O	142	2.92
3ELW	ASP	O	146	3.40
3G89	ALA	O	159	3.12
3G89	HOH	O	425	3.22
3G89	HOH	O	948	3.25
3G89	HOH	O	955	3.38
3G89	HOH	O	686	3.47
3GCZ	ASP	O	146	3.17
3IHT	GLY	O	114	3.53
3KKZ	GLN	O	26	2.83
3KKZ	HOH	O	777/701	3.28
3M6W	HOH	O	985	3.32
3M6W	HOH	O	984	3.41
3MB5	HOH	O	267	3.28
3MB5	ASP	OD2	169	3.40
3MB5	GLN	O	75	3.53
3MTE	PHE	O	105	3.02
3NDI	HOH	O	481	3.56
3NDI	HOH	O	482	3.56
3NDI	HOH	O	480	3.66
3OOI	HOH	O	247	3.11
3OOI	TYR	OH	207	3.49
3P97	HOH	O	343	2.30
3P97	HOH	O	635	2.94
3P97	HOH	O	462	3.34
3P97	ASP	O	146	3.40
3PFG	HOH	O	485	3.39
3PFG	PHE	O	118	3.49
3PFG	TYR	OH	14	3.49
3QWP	SER	O	202	3.08
3QWP	ASN	OD1	181	3.25
3QWP	TYR	OH	239	3.34
3RFA	GLY	O	177	3.26
3RQ4	PHE	O	160	3.22
3RQ4	HOH	O	267	3.34
3RQ4	TYR	OH	217	3.34
3S8P	PHE	O	250	3.10
3S8P	ALA	O	269	3.18
3S8P	TYR	OH	307	3.40
3UJ7	ASP	O	128	2.85
4HTF	HOH	O	459	3.21
3TM4	ASN	OD1	293	3.47

Table S1: AdoMet methyl CH···O hydrogen bond distances for all high-resolution (<2.00 Å) methyltransferase•AdoMet crystal structures in PDB. For structures with multiple copies within the PDB file, C···O distances were averaged between chains. The only methyltransferases that did not display methyl CH···O hydrogen bonds (accession codes 1VPT and 4DF3), in which the closest AdoMet methyl C···O distances were 3.70 Å, and 3.33 Å, respectively. *BIE is the catechol-o-methyltransferase inhibitor BIA 8-176.

	SET7/9 Y335F•TAF10•AdoHcy	SET7/9•TAF10 K189A•AdoMet	SET7/9•TAF10 K189A•AdoHcy
PDB Code	4J7I	4J83	4J8O
Data collection			
Space group	$P3_221$	$P3_221$	$P3_221$
Cell dimensions			
a, *b*, *c* (Å)	82.3, 82.3, 95.3	83.5, 83.5, 95.8	87.2, 87.2, 94.2
α,*β*,*γ* (°)	90, 90, 120	90, 90, 120	90, 90, 120
Resolution (Å)	50-2.56(2.62-2.56)	50.00-1.70(1.74-1.70)	50.00-1.63(1.67-1.63)
R_{merge} (%)	10.5(51.6)	7.1(48.3)	6.3(56.2)
I/sI	15.5(2.0)	27.4(7.1)	30.5(4.9)
Completeness (%)	97.8(84.4)	99.9(100)	99.9(100)
Redundancy	3.8(3.2)	11.1(11.1)	11.1(11.1)
Refinement			
Resolution (Å)	2.56	1.70	1.63
No. of Reflections	12438	40793	48994
R_{work}/ R_{free}	0.20/0.26	0.19/0.21	0.19/0.23
No. of Atoms	1868	2148	2228
Protein	1838	1935	1920
Ligand/ion	25	66	76
Water	5	147	232
B-factors	44.2	24.8	23.8
Protein	46.9	24.6	23.2
Ligand/ion	71.1	31.5	27.9
Water	37.6	34.3	34.2
R.M.S Deviations			
Bond lengths (Å)	0.014	0.015	0.015
Bond angles (°)	1.38	1.52	1.51
MolProbity Score			
Percentile	94%	87%	92%
Resolution Range (Å)	2.56± 0.25	1.70 ± 0.25	1.63 ± 0.25
Ramachandran			
Favored (%)	93.0	96.3	95.9
Allowed (%)	7.0	3.7	4.1
Outliers (%)	0	0	0

Table S2: Crystallographic and refinement statistics for the structures of SET7/9 Y335F•TAF10•AdoHcy, SET7/9•TAF10 K189A•AdoHcy, and SET7/9•TAF10 K189A•AdoMet.